

1 *Journal of Geotechnical and Geological Engineering*

2 Special Issue on “Thermo-mechanical Response of Soils, Rocks, and Energy Geostuctures”

3

4 **Analysis of friction induced thermo-mechanical stresses on a heat exchanger pile in**
5 **isothermal soil**

6

7
8 **Tolga Y. Ozudogru**, Istanbul Technical University, Department of Civil Engineering / Virginia
9 Polytechnic Institute and State University, Via Department of Civil and Environmental
10 Engineering, ozudogru@itu.edu.tr

11 **C. Guney Olgun**, Virginia Polytechnic Institute and State University, Via Department of Civil
12 and Environmental Engineering, colgun@vt.edu

13 **Chloé F. Arson**, Georgia Institute of Technology, School of Civil and Environmental
14 Engineering, chloe.arson@ce.gatech.edu

15

16

17

18

19

20

21

22

23

24

25

26

27

28

29

30

31

32

33

34

35

36

37

38

39

40

41

42

43

44

45

46

47

48

49

50

51

52

53

54

55

56

57

58

59

60

61

62

63

64

65

Abstract. In most analytical and numerical models of heat exchanger piles, strain incompatibilities between the soil and the pile are neglected, and axial stresses imposed by temperature changes within the pile are attributed to the thermal elongation and shortening of the pile. These models incorporate thermo-hydro-mechanical couplings in the soil and within the pile foundation, but usually neglect thermo-mechanical couplings between the two media. Previous studies assume that the stress changes imposed by temperature variations in a heat exchanger pile are mainly due to the constrained thermal elongation and shortening of the pile. Also, several recent approaches utilize spring models that focus only on the soil-pile interface in modeling temperature-induced stresses in a heat exchanger pile and implicitly ignore the effect of the full displacement field on soil-pile interaction. By contrast, in this paper, interface elements are introduced in a numerical model of a heat exchanger pile, analyzed in axisymmetric and stationary conditions. The pile is subjected to a uniform temperature increase, with free top and fixed top conditions in elastic and elasto-plastic soil profiles. Simulation results show that the constrained vertical elongation is the most detrimental factor for pile foundation performance. However it is worth noticing that while mechanical constraints (e.g., fixed top and/or fixed bottom) impose maximum stress increases at the ends of the pile, interface effects result in maximum stresses around the mid-length of the pile. This preliminary study indicates that soil-pile friction does not increase pile internal stresses to the point where it would be necessary to over-dimension the foundation pile for heat exchanger use. Furthermore, one cannot expect a significant gain in foundation performance due to the improvement of soil-pile frictional resistance as a result of increased lateral stresses at soil-pile contact. Additional numerical analyses are ongoing, in order to investigate the role of the degree of fixity induced by the building on the heat exchanger pile, and to extend these preliminary analyses to transient operational modes and cyclic thermo-mechanical loading of the heat exchanger pile.

Keywords: heat exchanger pile; finite element analysis; interface; friction; thermo-mechanical stress; numerical modeling.

4 **1. Introduction**

5
6
7 In a heat exchanger pile, the temperature gradient between the ground and the pile can be utilized
8 for heat transfer between the ground and the deep foundation. Thermal energy is extracted from
9 the ground in heating mode, and is injected into the ground in cooling mode with the use of the
10 heat carrier fluid circulating in the tubing system embedded in the pile (Brandl, 2006; Adam and
11 Markiewicz, 2009). Heat transfer around a heat exchanger pile can be modeled in the same way
12 as thermal diffusion around a geothermal borehole (Arson et al., 2013; Ozudogru et al., 2014),
13 however thermo-mechanical couplings need to be accounted for to predict the interactions
14 between a heat exchanger pile and the surrounding soil. So far, thermo-mechanical couplings
15 were modeled separately for the pile and for the surrounding soil.
16
17

18
19 Temperature-controlled triaxial tests performed on saturated kaolin samples evidenced that
20 temperature increase causes normally consolidated soils to harden (i.e., modulus increase)
21 (Cekerevac and Laloui, 2004). Normally consolidated clays tend to contract with heating, while
22 overconsolidated clays dilate during heating. In addition, it was shown that the slope of the
23 critical state line is independent of temperature, the hydrostatic yield limit (preconsolidation
24 pressure) decreases with heating, and shear strength tends to increase with temperature (Leroueil
25 and Marques, 1996). A thermo-mechanical elasto-plastic model was later proposed for soils
26 subjected to cyclic temperature changes (Laloui and Cekerevac, 2008). Thermal shear hardening
27 was also observed by comparing cyclic loading tests performed at ambient and elevated
28 temperatures (Cekerevac and Laloui, 2010).
29
30

31
32 Thermo-hydro-mechanical soil and concrete constitutive models were implemented in several
33 finite difference and finite element codes. In most cases, the pile is modeled as a thermo-elastic
34 solid, and the ground is assumed to follow a thermo-poro-elastic behavior (Laloui et al., 2006;
35 Bourne-Webb et al., 2009; Li and Zheng, 2009; Li et al., 2010; Raymond et al., 2011; Diersch et
36 al., 2011; Amatya et al., 2012). A recent study by the authors showed that the increase in contact
37 pressure induced by radial thermal expansion of the pile is small in magnitude and therefore
38 would not result in significant increases in shaft resistance (Olgun et al., 2014). Free body
39 diagrams based on one-dimensional thermo-elasticity can explain pile longitudinal contraction in
40 heat extraction mode and pile longitudinal extension in heat injection mode (Bourne-Webb et al.
41 2009). The resulting vertical deformation of the pile causes differential displacements at the
42 interface between the pile and the soil, and thus, develops friction at the soil-pile interface. More
43 sophisticated numerical models used to study the interaction between heat exchanger piles and
44 the surrounding soil mass focus on material properties and fluid flow in the tubes. For instance,
45 Abdelaziz et al. (2011) studied the influence of ground thermal conductivity, grout
46 characteristics, flow pipe diameter, flow rate and heating power on the temperature distribution
47 around a heat exchanger pile. Water content of the soil around the pile can also impact heat
48 exchanger pile operation as the thermal conductivity is strongly influenced by the degree of
49 saturation. Fan et al. (2007) showed that the degree of soil saturation and ground water flow
50 influence the heat transfer between a heat exchanger pile and the surrounding soil.
51
52
53
54
55

56
57 Interface elements combining non-linear stiffness components with sliders and dilatant
58 components were employed to mimic the behavior of granular media in simple shear at the
59 interface with the pile (Comodromos and Bareka, 2005). Thin elements were employed to model
60
61

4 shaft friction and the effects of localized shear around cast-in-place piles (Lee and Long, 2008;
5 Liu et al., 2012). Contact mechanics was also used in large deformation to simulate pile
6 installation (Fischer et al., 2007), and quantitative experimental data was recently obtained to
7 characterize the shear behavior of soil/steel interfaces subjected to large displacements (Ho et al.,
8 2011). However, despite experimental evidence brought on the development of shear stresses at
9 the interface between heat exchanger piles and the ground (McCartney and Rosenberg, 2011;
10 Suryatriyastuti et al., 2012), no model was proposed to account for the evolution of friction
11 resistance with temperature variation in a heat exchanger pile. This implies that the
12 displacements of the soil in contact with the pile follow the slip displacements of the outer
13 surface of the pile, and therefore, the thermal strain incompatibilities between the soil and the
14 pile can be neglected. The impact of slip displacements along the pile on soil shear strength has
15 never been quantitatively assessed so far.
16
17
18
19

20 In this paper, a mechanical interface model is utilized to account for the discontinuities and slip
21 displacements that may occur between the soil and the heat exchanger pile. A model problem of
22 heat exchanger pile is studied with the finite element method, in stationary axisymmetric
23 conditions. Contrary to the current models available to predict internal thermo-mechanical
24 stresses in a heat exchanger pile, an interface element is used to interpret slip displacements and
25 shear stresses along the pile/soil contact surface of a free-top floating pile subject to prescribed
26 elevated temperatures (Section 2). In order to understand the impact of the degree of fixity
27 induced by the constraint of the soil in contact with the pile, a parametric study on soil strength is
28 presented in Section 3. Interface effects are also studied for a fixed-top floating pile, and the
29 impact of pile temperature increase on the performance of the foundation is discussed.
30
31
32
33
34
35
36
37
38
39
40
41
42
43
44
45
46
47
48
49
50
51
52
53
54
55
56
57
58
59
60
61
62
63
64
65

4 **2. Thermo-mechanical stresses induced by friction on a heated pile floating in an** 5 **isothermal soil mass** 6

7 **2.1. Numerical model** 8 9

10 The goal of this numerical study is to determine whether the reaction of the soil mass plays a
11 significant role on the thermo-mechanical performance of heat exchanger piles. Emphasis is
12 placed on the thermo-mechanical stresses developed in the pile upon temperature increase. In
13 practice, the steady state distribution of temperatures within a cross section of a heat exchanger
14 pile equipped with a U-tubing system is indeed uniform, and the maximum temperature
15 difference between the top and bottom of the pile does not exceed a few degrees (Bourne-Webb
16 et al., 2009; Laloui et al., 2006). Former studies also indicate that the gradients of temperature
17 expected in the soil mass upon heating and cooling cycles amount to a few degrees only (Brandl,
18 2006; Katzenbach et al., 2008). Accordingly, it is assumed that temperature within the pile is
19 uniformly distributed. Since the present study focuses on the transmission of shear stress
20 between the soil and the pile, heat diffusion within the soil around the pile is neglected: the soil
21 is modeled as a reservoir that remains at a constant temperature. Even though this assumption
22 seems limited compared to the actual processes in the field, it allows the uncoupling of soil-pile
23 interaction from soil dilation and helps us study soil-pile shear transfer in the context of
24 temperature-induced pile elongation.
25
26
27
28
29

30 The finite element model used in the analyses was built with COMSOL Multiphysics™ software
31 (COMSOL, 2013), in stationary and axisymmetric conditions (dimensions are indicated in
32 Figure 1). The top of the pile is either free (Sections 2 and 3.1) or fixed (Section 3.2). The soil is
33 free of stress at the top of the domain and fully fixed at the bottom of the model. In the far field,
34 geostatic stress conditions are assumed with roller boundary condition on the right hand side
35 boundary. The left hand side boundary represents the axis of symmetry of the domain. The heat
36 exchanger pile is modeled as a thermo-elastic concrete cylinder embedded in either a perfectly
37 elastic or an elasto-plastic soil mass governed by Mohr-Coulomb yield criterion. Spring elements
38 are used at the pile toe to model the normal reaction of the soil. Interface elements are used in
39 order to model the tangential reaction of the soil on the pile shaft. The normal contact law is
40 linear elastic, and the tangential contact law is elastic-perfectly plastic, as illustrated in Figure 2.
41 The interface shear strength is assumed to be equal to that of the soil.
42
43
44
45

46 Table 1 summarizes the main constitutive equations used in the numerical model. Material
47 parameters assigned to the pile, the soil and the interface are listed in Table 2 and Table 3. The
48 mesh shown in Figure 3 consists of 41,318 finite elements. Initially, both the soil and the pile are
49 set at a temperature of 15°C. The temperature of the pile is uniformly increased by increments of
50 1°C, up to a temperature of 40°C.
51
52

53 **2.2. Internal stresses in a free-top heated pile embedded in elastic soil** 54

55 First, the system is analyzed when the soil is perfectly elastic with a Young’s modulus $E = 50$
56 MPa. The pile is subjected to the normal reaction of the soil at the toe, and to normal and
57 tangential reaction on the shaft. As a result, the vertical strain of the pile is less than that of a free
58 pile (Figure 4), which would be equal to the product of the thermal expansion coefficient ($\alpha = 10$
59
60
61
62
63
64
65

4 $\mu\epsilon/^\circ\text{C}$) and the temperature change ($\Delta T = 25^\circ\text{C}$). The pile at mid-depth would undergo a strain of
5 250 $\mu\epsilon$ if it was free to expand as indicated by the thermal strain in the pile as shown in Figure 4.
6 The mechanical strain in the pile ($\epsilon \sim -32 \mu\epsilon$) is indicative of the compressional strains as a result
7 of the constraint from the shear resistance of the soil at the interface in reaction to the
8 temperature-induced pile elongation. As a result, the total strain in the pile (total strain = thermal
9 strain + mechanical strain) is equal to $\sim 218 \mu\epsilon$ because of the induced compressional mechanical
10 strain in reaction to the soil resistance.
11
12

13
14 It is verified that vertical stress in the soil does not change upon pile temperature increase (Figure
15 5), which is consistent with the assumptions made in the numerical model: the soil does not
16 undergo any thermo-mechanical stress changes since soil temperature is maintained constant.
17 Therefore, the vertical heave deformations noted in the soil at the vicinity of the heated pile are
18 induced by a purely mechanical effect: the soil is dragged by friction against the pile outer
19 surface as the pile undergoes temperature-induced elongation. This can be verified by comparing
20 the vertical displacement of the soil and the pile at soil-pile contact (Figure 6) with the slip
21 displacement along the interface at that point (Figure 7). For example, at mid-depth of the pile (z
22 = 10 m), the slip displacement due to drag slightly exceeds 0.095 mm for a 25°C temperature
23 increase, where the vertical pile displacement is about 0.179 mm at that depth compared with the
24 soil displacement of 0.084 mm. These results also demonstrate the importance of assuming
25 constant soil temperature as the soil-pile interaction due to pile elongation is isolated and these
26 effects can be observed in the absence of temperature-induced soil deformations.
27
28
29
30

31 Figures 8 shows that finite fixity at the pile toe not only counteracts thermal elongation of the
32 pile, but also narrows the zone of the pile subjected to downward displacement ($z = 10.7 \text{ m} > 10$
33 m). The top part of the pile ($z < 10.7 \text{ m}$) tends to expand upwards upon temperature increase,
34 while the lower segment of the pile expands downward (Figure 8). The neutral point at around
35 where the pile elongates upwards and downwards would be at mid-length of the pile if the pile
36 was expanding freely in the absence of any soil. However in this particular example, the point of
37 inversion where the temperature-induced pile deformations transition from upward to downward
38 (i.e. the neutral point) is located at a depth of $z = 10.7 \text{ m}$ as seen in Figure 8. Soil reaction at the
39 pile toe in addition to the shear resistance along the pile shaft causes the neutral point to
40 propagate to levels deeper than mid-length of the pile. The neutral point also represents where
41 the opposing soil resistances along the upward and downward segments of the pile are balanced.
42 Consequently, the compressional stress due to pile elongation and the associated soil resistance is
43 maximized at the neutral point where thermo-mechanical shear stresses acting on the pile reverse
44 from downward to upward along the pile length. The thermo-mechanical stress distribution
45 would be symmetrical if the pile was free at both ends for an elastic soil with uniform stiffness
46 throughout. Stress distributions for different levels of temperature increase in the analyses are
47 shown in Figure 9 and it is seen that the compressional stress along the pile achieves a maximum
48 value of 552.9 kPa at $z = 10.7 \text{ m}$ depth.
49
50
51
52
53

54 **2.3. Interface behavior - elastic soil**

55

56
57 Aside from the pile ends, the total normal stress at the interface equals the radial thermo-
58 mechanical stress developed in the pile. For the elastic soil case, the interface contact is linear
59 elastic in both directions; normal stiffness and tangential stiffness being 100 MPa/m and 10
60

4 MPa/m, respectively. Normal stress increase at the soil-pile interface is small and remains in the
5 order of a few kilopascals (Figure 10). This is an important observation suggesting that the
6 normal stress changes at the pile-soil interface are likely to be small and therefore temperature
7 changes will not have a significant influence on pile capacity (Olgun et al., 2014). Slip
8 displacement along the interface remains in the order of a few millimeters (Figure 11), consistent
9 with the small magnitude of deformation difference between the pile and the soil at mid-length
10 of the pile (Figure 6). The linear relationship between slip displacement and interface shear stress
11 is reflected in Figure 11 and Figure 12. The distribution of shear stress along the interface
12 follows a trend opposite to that of slip. Moreover, it can be verified that the amount of shear
13 stress mobilized along the soil-pile interface is equal to the product of the tangential interface
14 stiffness and the slip displacement (in agreement with the model), which amounts to a maximum
15 of less than 20 kPa for a temperature increase of $\Delta T = 25^\circ\text{C}$. The comparison of Figure 8 and
16 Figure 12 allows the verification of the balance of axial forces on any portion of the pile:
17

$$\pi r^2 \sigma_a(z) = \pi r^2 \sigma_a(z=0) + 2\pi r \int_0^z \tau(z') dz' \quad (1)$$

18 The equation above shows that the shear stress mobilized at the interface is balanced by the axial
19 stress developed within the pile. Recommendations made in previous thermo-mechanical
20 analyses (Laloui et al., 2006) indicate that floating heat exchanger piles typically need to be
21 reinforced near the top of the pile, in order to support the additional stresses induced by
22 temperature increase. This is particularly important for piles constrained at the top in the
23 presence of a structure as opposed to the pile analyzed above. Additional analyses are presented
24 below where fixity of the pile top is investigated.
25

26 **2.4. Validation of the numerical model by a field test**

27 The finite element model presented above was validated using the measurements from the field
28 test presented by Amatya et al. (2012). This field test was located at Lambeth College in South
29 London. The test setup included a mechanically loaded heat exchanger pile and a heat sink pile.
30 The main test pile and the heat sink pile were subjected to reverse thermal operations, such that
31 when the main test pile was cooled down, the heat sink pile was heated with the heat extracted
32 from the main pile.
33

34 Data collected for the heat sink pile was used for model validation. The pile had a diameter of 55
35 cm and a length of 30 m. The head of the heat sink pile was free and had no mechanical load or
36 constraint. The drilling log indicated that the first 4 m of the soil profile consisted of granular fill
37 and sand and gravel layer, underlain by a stiff, fissured silty clay layer. The clay layer extended
38 below the toe of the pile. The strength parameters were evaluated solely from standard
39 penetration test (SPT) data and it was observed that the undrained soil strength increased with
40 depth (Figure 13a).
41

42 The Young's modulus of the concrete was 40 GPa and the coefficient of thermal expansion was
43 $8.5 \mu\epsilon/^\circ\text{C}$. During the field test, strain and temperature data were continuously measured with
44 optical fiber sensors (OFS) in addition to strain gauges at discrete elevations within the pile. The
45 heat sink pile was subjected to a temperature increase of 29.4°C and it was observed that the
46 temperature change was uniform along the entire length of the pile. The strain data was used to
47

4 evaluate an idealized axial load profile (Figure 14b) and the shear stress along the pile-soil
5 interface was interpolated using this idealized profile (Figure 14c).
6

7
8 For validation purposes, three finite element analyses were performed with different Young’s
9 modulus to shear strength ratios (E/S_u) and for different slip displacements at fully mobilized
10 shaft resistance. Details are given in Table 4 and shown in Figure 13. The geometry and the
11 mesh were similar to those presented in the preceding sections. Pile temperature was gradually
12 and uniformly increased to achieve a temperature increase of 29.4°C in reference to the initial
13 pile and soil temperature.
14
15

16 The results of the numerical analyses are presented in Figure 14, along with the field
17 measurements. It can be seen that, Analysis 3 captures the peak axial strain while Analysis 1 has
18 a better fit of the average (Figure 14a). The field data shows that the strain values measured near
19 the ends of the pile (e.g., the first and the last 4 m) are slightly higher than the free thermal strain,
20 which is theoretically impossible. Figure 14b shows the evaluated pile axial load with respect to
21 depth. It can be inferred that the value of the peak axial load is approximately predicted by
22 Analysis 2, but the general behavior of the pile axial load is best captured by Analysis 3. It is not
23 practical to compare the shear stress distribution along the pile-soil interface since it was
24 interpolated using the idealized axial load profile. On the other hand, the neutral point provided
25 by Analysis 3 is the only one which agrees with the field measurements (Figure 14c). Overall, it
26 can be concluded that the finite element modeling approach presented in this study works well in
27 simulating thermo-mechanical behavior of a heat exchanger pile under temperature changes.
28 These results also highlight the importance of soil and interface parameters on the results.
29
30
31
32
33

34 **3. Parametric analyses**

35 **3.1. Influence of soil strength on the thermo-mechanical stress induced by friction in a** 36 **heated pile floating in isothermal soil** 37 38

39 The previous analysis shows that slip displacements between a heated pile and the surrounding
40 soil are small in magnitude and the maximum value of the shear stress mobilized at the interface
41 is in the order of 16 kPa near the pile top for a temperature increase of 25°C. In order to study the
42 impact of potential soil yielding on the mechanical performance of the heat exchanger pile,
43 simulations were repeated for an elasto-plastic soil, for the following shear strengths: $S_u = 25\text{kPa}$,
44 50kPa and 100 kPa, instead of the elastic soil discussed in Section 2. Young’s modulus of the
45 soil in different sets of parametric analyses was varied to maintain a modulus to shear strength
46 ratio $E/S_u = 500$. The stiffness and the yield limit of the tangential spring in the interface
47 elements were varied accordingly (Table 1). The other material parameters, the mesh, the initial
48 conditions and the boundary conditions are kept the same as in Section 2.
49
50
51
52

53 The difference between the tangential displacement of the pile and that of the soil along the
54 interface are shown in Figure 15. The resulting shear stress distributions for the three soil
55 strength cases and the elastic case are shown in Figure 16. The magnitude of the slip
56 displacement at the soil/pile interface (i.e. difference in tangential displacement between soil and
57 the pile) is very similar for the different soil models. In fact, the distribution of slip displacement
58 for the case with $S_u = 100\text{ kPa}$ is almost identical to the case with elastic soil. Moreover, the
59
60
61
62
63
64
65

4 shear stress distributions for different cases vary in proportion to soil modulus for different cases.
5 Figure 17 shows that the variation of axial stress in the pile is almost proportional to the stiffness
6 of the tangential spring in the interface. For instance, the values of peak axial stress at $z = 10.7$ m
7 are 150.6 kPa, 292.5 kPa and 552.9 kPa for the soils with $S_u = 25, 50$ and 100 kPa, respectively.
8 The ratios of the maximum axial stresses with respect to the $S_u = 100$ kPa soil are 0.27/0.53/1.00
9 for $S_u = 25, 50$ and 100 kPa, respectively. It is seen that the magnitude of shear stresses and axial
10 pile stresses are almost proportional to the stiffness of the soil-pile interface, which is directly
11 correlated to soil strength and stiffness in this model. Moreover, the axial stress in the pile for
12 $S_u = 100$ kPa case is almost identical to the case with pile in elastic soil. The amount of slip at
13 the interface is always below 1 cm, which implies that the interface remains elastic for all the soil
14 conditions investigated. Similar conclusions can be drawn from the variations of strains within
15 the pile (not shown herein for the sake of brevity). While thermal strains remain at the same
16 value for the four cases for a given temperature increase, mechanical strains increase almost
17 linearly with soil shear strength. This is related to the same phenomenon described above.
18 Identical piles in soils with different strengths undergo similar thermal strains in response to a
19 given temperature increase. However, the mechanical strains are manifested in proportion to the
20 interface strength in the corresponding soil mass with a given soil strength and stiffness.
21
22
23
24
25

26 **3.2. Influence of the pile fixity on the thermo-mechanical stresses induced by friction in a** 27 **heated pile floating in isothermal soil** 28

29
30 The four simulations above were repeated for an identical pile fixed at the top in order to
31 determine the effect of a building on the temperature-induced stress increases within a heat
32 exchanger pile. It is quite conceivable that the constraint from a building would impose a
33 different displacement field along the pile, which will directly influence the development of slip
34 displacements and shear stresses along the pile length. In these analyses, displacements at the top
35 of the pile were fully fixed, which represents an end-case in comparison to a building with a
36 foundation that will provide some degree of constraint but will still have some finite stiffness.
37 All the other properties of the numerical model were kept the same as in Sections 2 and 3.1.
38
39
40

41 The main effect of heating a pile with a fixed top is the concentration of compressional stresses
42 near the top of the pile, due to the mechanical boundary conditions imposed on the pile. In this
43 case, soil friction plays a minor role compared to the constrained vertical elongation of the pile
44 due to the fixity at pile top. The maximum values of compressional stress increase near the top of
45 the pile due to heating are 1157.5 kPa, 1582.2 kPa and 2228.4 kPa for the soils with $S_u = 25, 50$
46 and 100 kPa, respectively (Figure 18). Similarly, the pile in elastic soil behaves almost identical
47 compared to the pile within the soil with $S_u = 100$ kPa.
48
49

50
51 It is also seen that some level of tensile stresses develops near the top of the pile, presumably as a
52 result of the soil heave from the upward deformations of the soil at the lower levels. Upward slip
53 of the soils near the ground surface relative to the fixed pile top and the associated shear stresses
54 result in tensile stresses near the top of the pile. Shear stresses along the interface are negative
55 and act upward within a very narrow zone, up to about 1.5 m depth (Figure 19). This is
56 demonstrated by the slip displacements which are negative within the top 1.5 meters and positive
57 at deeper levels along the pile (Figure 20). This indicates that the soil around the pile tends to
58 displace upwards compared to the pile along the soil-pile interface at these upper levels. These
59
60
61

4 results show that heave of the soils near the top and the associated shear stresses along this
5 segment of the pile causes the development of tensile stresses. The displacement field within the
6 soil around the pile indicates that the upward displacement of the soils at the lower levels pushes
7 the soils near the top upwards. This secondary displacement field causes a relative upwards slip
8 displacement of the soil at the upper levels with respect to the pile with fixed top causing tensile
9 stresses along the pile. This underscores the importance of modelling the full displacement field
10 which would only be possible with an approach similar to the one presented in this study. Other
11 simpler approaches which employ springs to model soil-pile interface would not be able to
12 capture such a phenomenon related to the full displacement field and coupling of soil
13 deformations at different levels (Knelwolf et al., 2011).
14
15
16
17
18
19
20
21
22
23
24
25
26
27
28
29
30
31
32
33
34
35
36
37
38
39
40
41
42
43
44
45
46
47
48
49
50
51
52
53
54
55
56
57
58
59
60
61
62
63
64
65

4 **4. Conclusions**

5
6 Analytical and numerical models of heat exchanger piles incorporate thermo-hydro-mechanical
7 couplings in the soil and within the pile foundation, but usually neglect thermo-mechanical
8 couplings between the two media. Previous studies therefore assumed that the stress changes
9 imposed by temperature variations in a heat exchanger pile are mainly due to the constrained
10 thermal elongation and shortening of the pile. Also, several recent approaches utilized spring
11 models that focused only on the soil-pile interface in modeling temperature-induced stresses in a
12 heat exchanger pile and implicitly ignored the effect of the full displacement field on soil-pile
13 interaction.
14
15

16
17 In this paper, a numerical model of heat exchanger pile was analyzed in axisymmetric and
18 stationary conditions. The pile was subjected to a uniform temperature increase, and the
19 surrounding soil was kept at a constant temperature. The stiffness of the interface element
20 between the two media was assigned to be dependent on soil shear strength. The heat exchanger
21 pile was first studied with a free top in order to investigate the magnitude of internal thermo-
22 mechanical stresses that develop in the pile in reaction to the induced temperature increase. The
23 analyses show that the soil-pile interaction is directly influenced by the interplay between the
24 thermal strains in the pile and the associated shear stresses that develop along the soil-pile
25 interface. In subsequent analyses, the top of the pile was fixed, and the finite element model was
26 used to compute the total stress increase imposed on the heat exchanger pile upon heating, due to
27 both the constrained thermal elongation and the mobilization of friction along the pile.
28
29
30
31

32 Simulation results show that the constrained vertical elongation is the most detrimental factor for
33 pile foundation performance. Pure interface effects induce internal stresses about ten times
34 smaller than the stresses observed at pile ends for the case in which mechanical constraint is
35 present. However it is worth noticing that while mechanical constraints (e.g., fixed top and/or
36 fixed bottom) require oversizing heat exchanger piles at the ends, interface effects require
37 additional reinforcing the pile at mid-depth. Interface deformations in both cases are relatively
38 small indicating that the interface deformations are likely to remain elastic and reversible in
39 response to cycles of temperature changes. The same trends (with opposite signs) are expected
40 upon pile cooling in terms of deformations and stresses along the pile. This preliminary study
41 shows that it may not be critical to account for pile friction in dimensioning heat exchanger piles
42 as structural constraint can play a more significant role.
43
44
45
46

47 Another observation from the analyses suggests that no significant gain of foundation
48 performance is achieved as a result of friction upon pile heating. This is evidenced by small
49 increases in normal stresses at the pile-soil interface as a result of increased pile temperatures,
50 and therefore having a minor effect on frictional strength between the pile and the soil. Further
51 numerical analyses are ongoing to study the role of the degree of fixity induced by the presence
52 of a building on the heat exchanger pile, and to extend these preliminary analyses to more
53 realistic transient operational modes and cyclic thermo-mechanical loading of the heat exchanger
54 pile.
55
56
57
58
59
60
61
62
63
64
65

4 **Acknowledgements**

5 The first and second authors would like to express their gratitude for the support by the National
6 Science Foundation under Grants No. CMMI-0928807 and CMMI-1100752. The first author is
7 also funded as a visiting scholar by the Turkish Council on Higher Education and Istanbul
8 Technical University. The financial support from these funding sources is greatly appreciated.
9
10
11
12
13
14
15
16
17
18
19
20
21
22
23
24
25
26
27
28
29
30
31
32
33
34
35
36
37
38
39
40
41
42
43
44
45
46
47
48
49
50
51
52
53
54
55
56
57
58
59
60
61
62
63
64
65

4 **References**

- 5
6 Abdelaziz SL, Olgun CG, Martin II JR (2011) Design and Operational Considerations of
7 Geothermal Energy Piles, Proceedings of Geo-Frontiers 2011, March 13-16, 2011,
8 Dallas, Texas
9
- 10 Adam D, Markiewicz R (2009) Energy from Earth-Coupled Structures, Foundations, Tunnels
11 and Sewers. *Géotechnique*, 59(3): 229-236
12
- 13 Amatyia BL, Soga K, Bourne-Webb PJ, Amis T, Laloui L (2012) Thermo-mechanical behavior
14 of energy piles, *Géotechnique*, 62, 6, 503-519
15
- 16 Arson C, Berns E, Akrouch G, Sanchez M, Briaud J-L (2013) Heat Propagation around
17 Geothermal Piles and Implications on Energy Balance, in: *Energy Book Series - Volume*
18 *#1: “Materials and processes for energy: communicating current research and*
19 *technological developments”*, A. Méndez-Vilas ed., Formatex Research Center,
20 ISBN(13): 978-84-939843-7-3, 628-635
21
- 22 Bourne-Webb PJ, Amatyia B, Soga K, Amis T, Davidson C, Payne P (2009) Energy Pile Test at
23 Lambeth College, London: Geotechnical and Thermodynamic Aspects of Pile Response
24 to Heat Cycles. *Géotechnique*, 59(3): 237-248
25
- 26 Brandl H (2006) Energy foundations and other thermo-active ground structures. *Géotechnique*,
27 56(2), 81-122.
28
- 29 Cekerevac C, Laloui L (2004) Experimental study of thermal effects on the mechanical
30 behaviour of a clay, *International Journal for Numerical and Analytical Methods in*
31 *Geomechanics*, 28: 209-228
32
- 33 Cekerevac C, Laloui L (2010) Experimental analysis of the cyclic behaviour of kaolin at high
34 temperature, *Géotechnique*, 60(8): 651-655
35
- 36 Comodromos EM, Bareka SV (2005) Evaluation of negative skin friction effects in pile
37 foundations using 3D nonlinear analysis, *Computers and Geotechnics*, 32, 210-221
38
- 39 COMSOL (2013) COMSOL Multiphysics™ v4.3b: User’s guide and reference manual.
40 COMSOL, Burlington MA
41
- 42 Diersch H-JG, Bauer D, Heidemann W, Rühaak W, Schätzl P (2011) Finite element modeling of
43 borehole heat exchanger systems. Part 1. Fundamentals, *Computers & Geosciences*, 37,
44 1122-1135
45
- 46 Fan R, Jiang Y, Yao Y, Shiming D, Ma Z (2007) A study on the performance of a geothermal
47 heat exchanger under coupled heat conduction and groundwater advection. *Energy*,
48 32(11), 2199-2209
49
- 50 Fischer KA, Sheng D, Abbo AJ (2007) Modeling of pile installation using contact mechanics and
51 quadratic elements, *Computers and Geotechnics*, 34, 449-461
52
- 53 Ho TYK, Jardine RJ, Anh-Minh N (2011) Large-displacement interface shear between steel and
54 granular media, *Géotechnique*, 61(3):221-234
55
- 56 Katzenbach R, Clauss F, Waberseck T, Wagner I (2008) Coupled Numerical Simulation of
57 Geothermal Energy Systems, Proceedings of the 12th International Conference of
58 International Association for Computer Methods and Advances in Geomechanics
59 (IACMAG), October 1-6, 2008, Goa, India
60
- 61 Knellwolf C, Peron H, Laloui L (2011) Geotechnical analysis of heat exchanger piles, *Journal of*
62 *Geotechnical and Geoenvironmental Engineering*, 137: 890-902.
63
64
65

- 4 Laloui L, Nuth M, Vulliet L (2006) Experimental and numerical investigations of the behaviour
5 of a heat exchanger pile, *International Journal for Analytical and Numerical Methods in*
6 *Geomechanics*, 30: 763-781
7
- 8 Laloui L, Cekerevac C (2008) Non-isothermal plasticity model for cyclic behaviour of soils,
9 *International Journal for Numerical and Analytical Methods in Geomechanics*, 32:437-
10 460
11
- 12 Lee S, Long JH (2008) Skin friction of drilled CIP piles in sand from pile segment analysis,
13 *International Journal for Numerical and Analytical Methods in Geomechanics*, 32, 745-
14 770
15
- 16 Leroueil S, Marques, MES (1996) Importance of Strain Rate and Temperature Effects in
17 *Geotechnical Engineering, Proceedings of ASCE National Convention, 1996,*
18 *Washington DC*, pp. 1-60.
19
- 20 Li Z, Zheng M (2009) Development of a numerical model for the simulation of vertical U-tube
21 ground heat exchangers, *Applied Thermal Engineering*, 29, 920-924
22
- 23 Li S, Yang W, Zhang X (2010) Soil temperature distribution around a U-tube heat exchanger in a
24 multi-function ground source heat pump system, *Applied Thermal Engineering*, 29:3679-
25 3686
26
- 27 Liu H, Song E, Ling HI (2006) Constitutive modeling of soil-structure interface through the
28 concept of critical state soil mechanics, *Mechanics Research Communications*, 33, 515-
29 531
30
- 31 Liu J, Gao H, Liu H (2012) Finite element analyses of negative skin friction on a single pile,
32 *Acta Geotechnica*, 7, 239-252
33
- 34 McCartney JS, Rosenberg JE (2011) Impact of Heat Exchange on Side Shear in Thermo-Active
35 Foundations, *Proceedings of Geo-Frontiers 2011, March 13-16, 2011, Dallas, Texas*
- 36 Olgun CG, Ozudogru TY, Arson CF (2014) Thermo-mechanical radial expansion of heat
37 exchanger piles and possible effects on contact pressures at pile-soil interface,
38 *Géotechnique Letters*, DOI: 10.1680/geolett.14.00018, Volume 4, Issue July-September,
39 August 2014, pp. 170-178.
40
- 41 Ozudogru TY, Olgun CG, Senol A (2014) 3D numerical modeling of vertical geothermal heat
42 exchangers, *Geothermics*, Vol. 51, pp. 312-324.
43
- 44 Raymond J, Frenette M, Léger A, Magni E, Therrien R (2011) Numerical Modeling of
45 Thermally Enhanced Pipe Performances in Vertical Ground Exchangers, *ASHRAE*
46 *Transactions*, 900-907
47
- 48 Suryatriyastuti ME, Mroueh H, Burlon S (2012) Understanding the temperature-induced
49 mechanical behavior of energy pile foundations, *Renewable and Sustainable Energy*
50 *Reviews*, 16, 3344-3354
51
52
53
54
55
56
57
58
59
60
61
62
63
64
65

4 **Table Captions**
5

6
7 **Table 1** Constitutive equations used in the numerical model for soil elements, concrete elements
8 (in the heat exchanger pile) and the interface elements
9

10 **Table 2** Material properties
11

12 **Table 3** Soil types and strength parameters
13

14 **Table 4** Input parameters used in the analyses for model validation
15
16
17
18
19
20
21
22
23
24
25
26
27
28
29
30
31
32
33
34
35
36
37
38
39
40
41
42
43
44
45
46
47
48
49
50
51
52
53
54
55
56
57
58
59
60
61
62
63
64
65

4 **Figure Captions**
5

6
7 **Fig. 1** Finite Element Model geometry and dimensions.
8

9 **Fig. 2** Stress-displacement behavior of the interface element.
10

11 **Fig. 3** Mesh adopted in the Finite Element model.
12

13
14 **Fig. 4** Components of vertical strains vs. radial distance at mid-pile depth ($z=10\text{m}$) ($\Delta T=25^\circ\text{C}$)
15 relative to $\Delta T=0^\circ\text{C}$, for an elastic soil.
16

17
18 **Fig. 5** Axial stress in the pile and vertical stress in the soil vs. radial distance at mid-pile depth
19 ($z=10\text{m}$) relative to $\Delta T=0^\circ\text{C}$, for an elastic soil.
20

21
22 **Fig. 6** Vertical displacement vs. radial distance at mid-pile depth ($z=10\text{m}$) relative to $\Delta T=0^\circ\text{C}$,
23 for an elastic soil.
24

25 **Fig. 7** Slip displacement at the pile-soil interface vs. temperature change relative to $\Delta T=0^\circ\text{C}$, for
26 an elastic soil.
27

28
29 **Fig. 8** Vertical displacement along the pile center axis relative to $\Delta T=0^\circ\text{C}$, for an elastic soil.
30

31 **Fig. 9** Axial stress along the pile relative to $\Delta T=0^\circ\text{C}$, for an elastic soil.
32

33
34 **Fig. 10** Normal stresses along the pile-soil interface relative to $\Delta T=0^\circ\text{C}$, for an elastic soil.
35

36 **Fig. 11** Slip displacements along the pile-soil interface relative to $\Delta T=0^\circ\text{C}$, for an elastic soil.
37

38
39 **Fig. 12** Shear stresses along the pile-soil interface relative to $\Delta T=0^\circ\text{C}$, for an elastic soil.
40

41 **Fig. 13** Soil and interface parameters along the depth: (a) Undrained shear strength, (b) Young's
42 modulus; (c) Tangential spring constant along the pile-soil interface.
43

44
45 **Fig. 14** Comparison of field test measurements and finite element analyses: (a) Axial strain along
46 the length of the pile; (b) Pile axial load along the depth; (c) Shear stress along the pile-soil
47 interface.
48

49 **Fig. 15** Slip displacements along the pile-soil interface relative to $\Delta T=0^\circ\text{C}$, for $\Delta T=25^\circ\text{C}$, in the
50 four soils considered in this study.
51

52
53 **Fig. 16** Shear stresses along the pile-soil interface relative to $\Delta T=0^\circ\text{C}$, for $\Delta T=25^\circ\text{C}$, in the four
54 soils considered in this study.
55

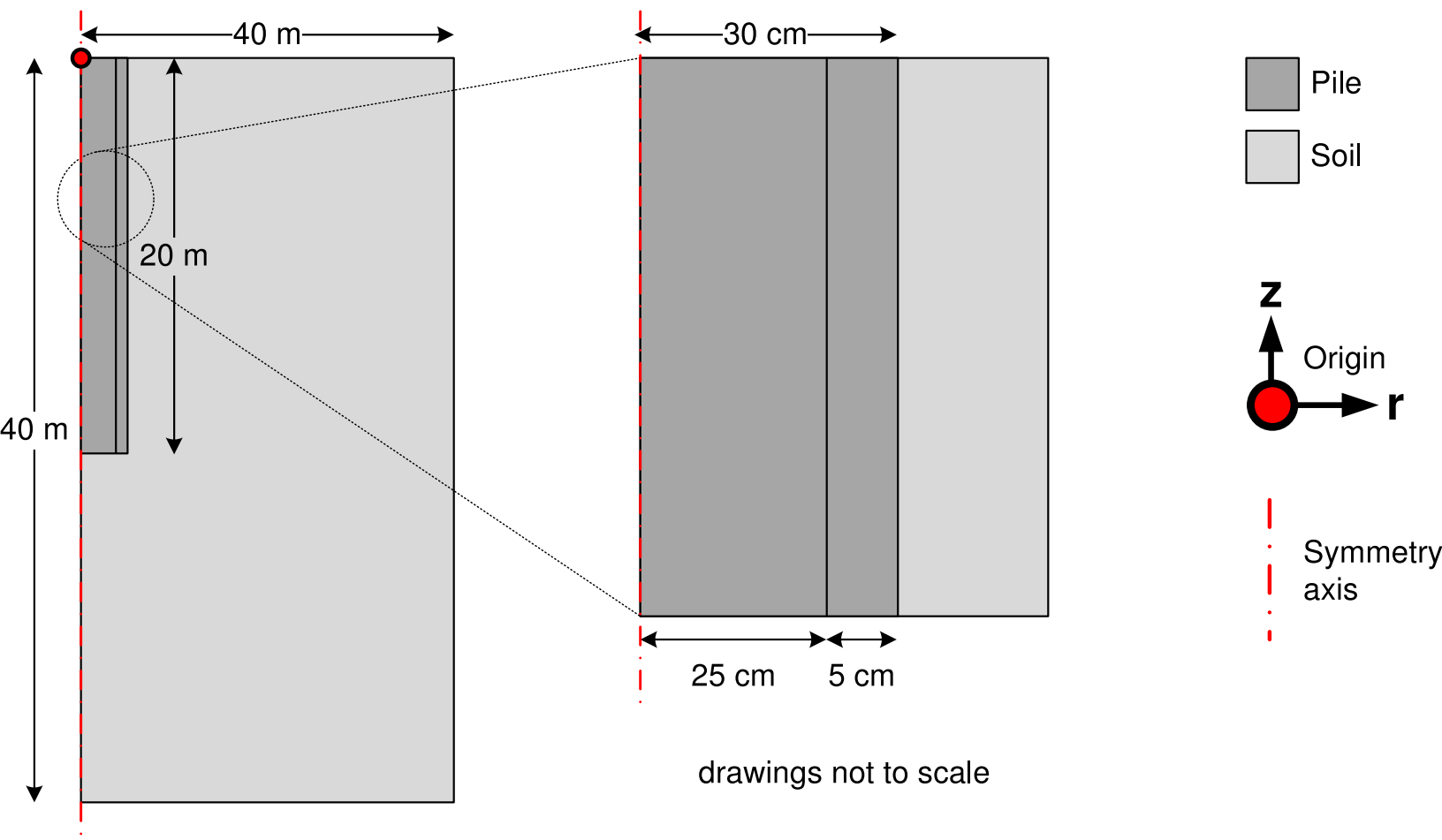
56
57 **Fig. 17** Axial stresses along the pile relative to $\Delta T=0^\circ\text{C}$, for $\Delta T=25^\circ\text{C}$, in the four soils
58 considered in this study.
59
60
61
62

4 **Fig. 18** Axial stresses along the pile relative to $\Delta T=0^{\circ}\text{C}$, for $\Delta T=25^{\circ}\text{C}$ (fixed top).
5

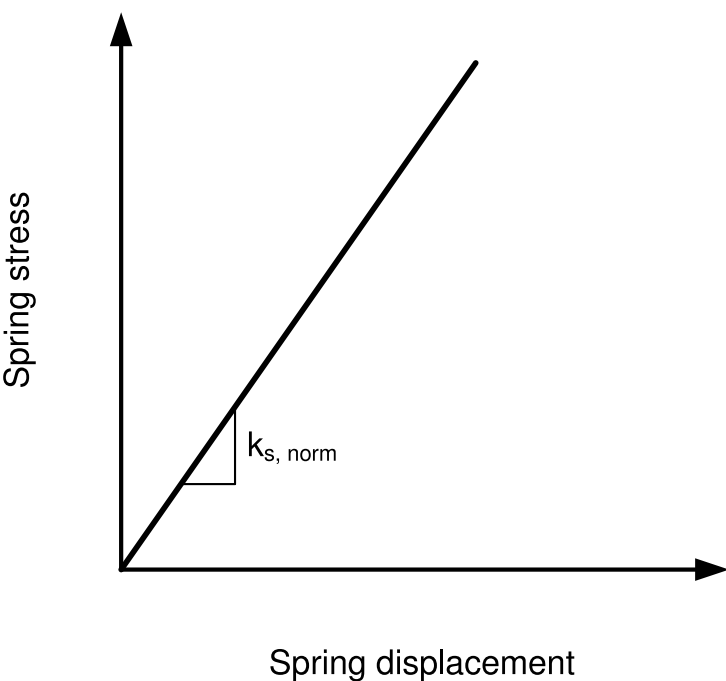
6 **Fig. 19** Shear stresses along the pile-soil interface relative to $\Delta T=0^{\circ}\text{C}$, for $\Delta T=25^{\circ}\text{C}$ (fixed top).
7

8 **Fig. 20** Slip displacements along the pile-soil interface relative to $\Delta T=0^{\circ}\text{C}$, for $\Delta T=25^{\circ}\text{C}$ (fixed
9 top).
10
11
12
13
14
15
16
17
18
19
20
21
22
23
24
25
26
27
28
29
30
31
32
33
34
35
36
37
38
39
40
41
42
43
44
45
46
47
48
49
50
51
52
53
54
55
56
57
58
59
60
61
62
63
64
65

Figure 1
[Click here to download Figure: Fig 1.eps](#)



a) Normal spring



b) Tangential spring

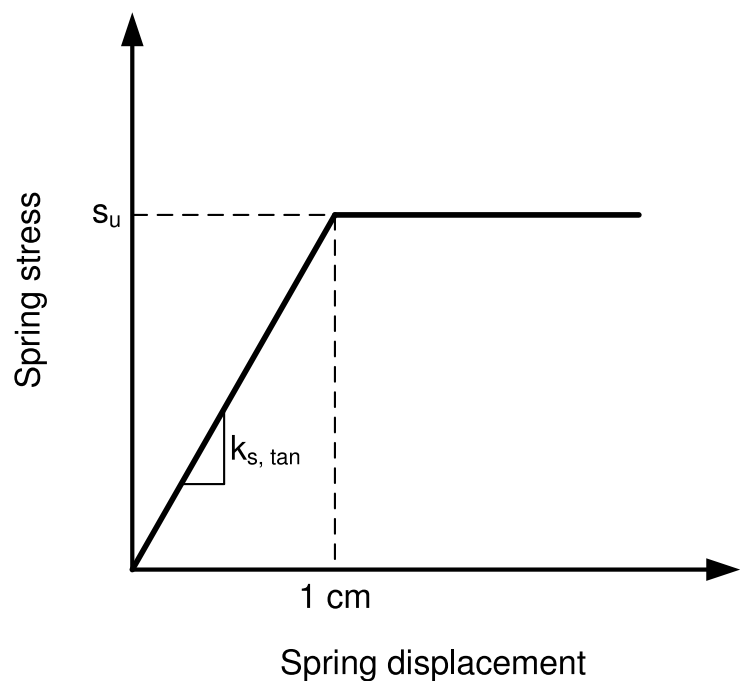


Figure 3
[Click here to download high resolution image](#)

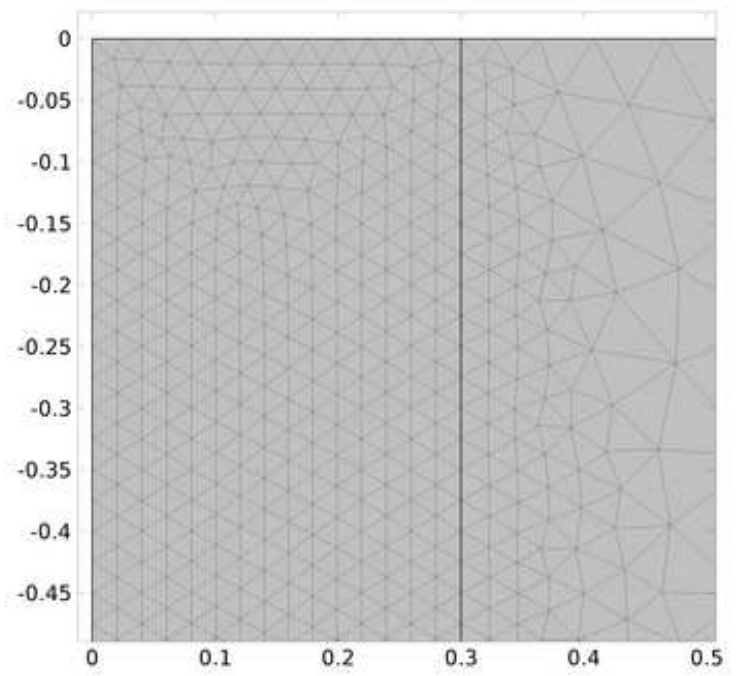
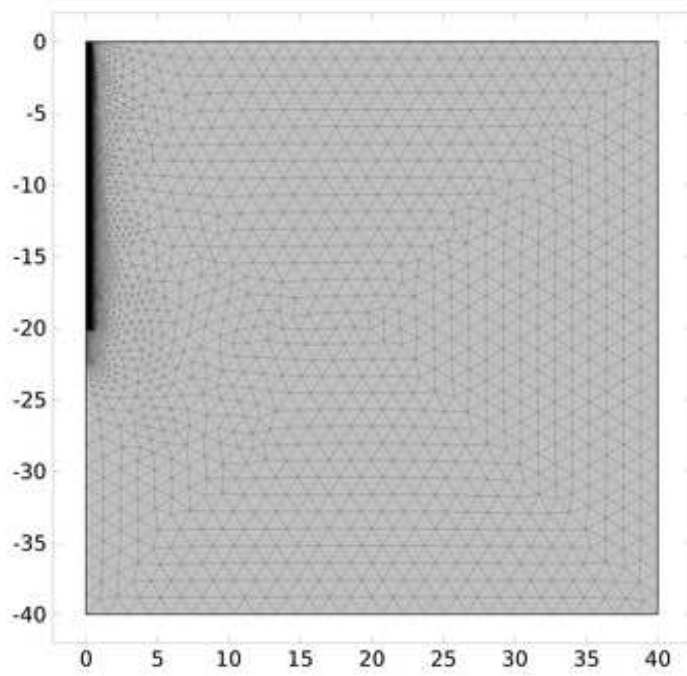


Figure 4
[Click here to download Figure: Fig 4.eps](#)

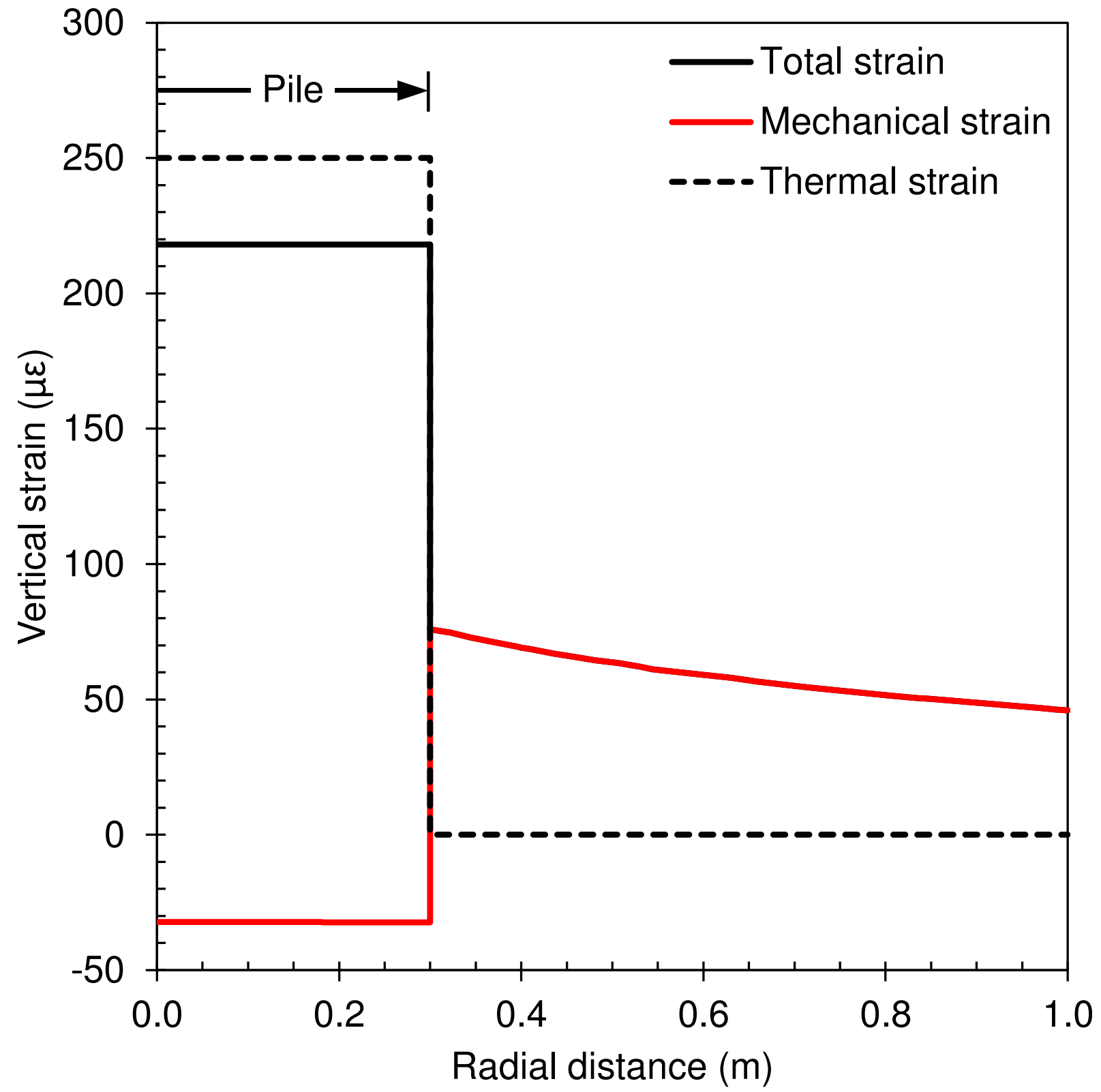


Figure 5
[Click here to download Figure: Fig 5.eps](#)

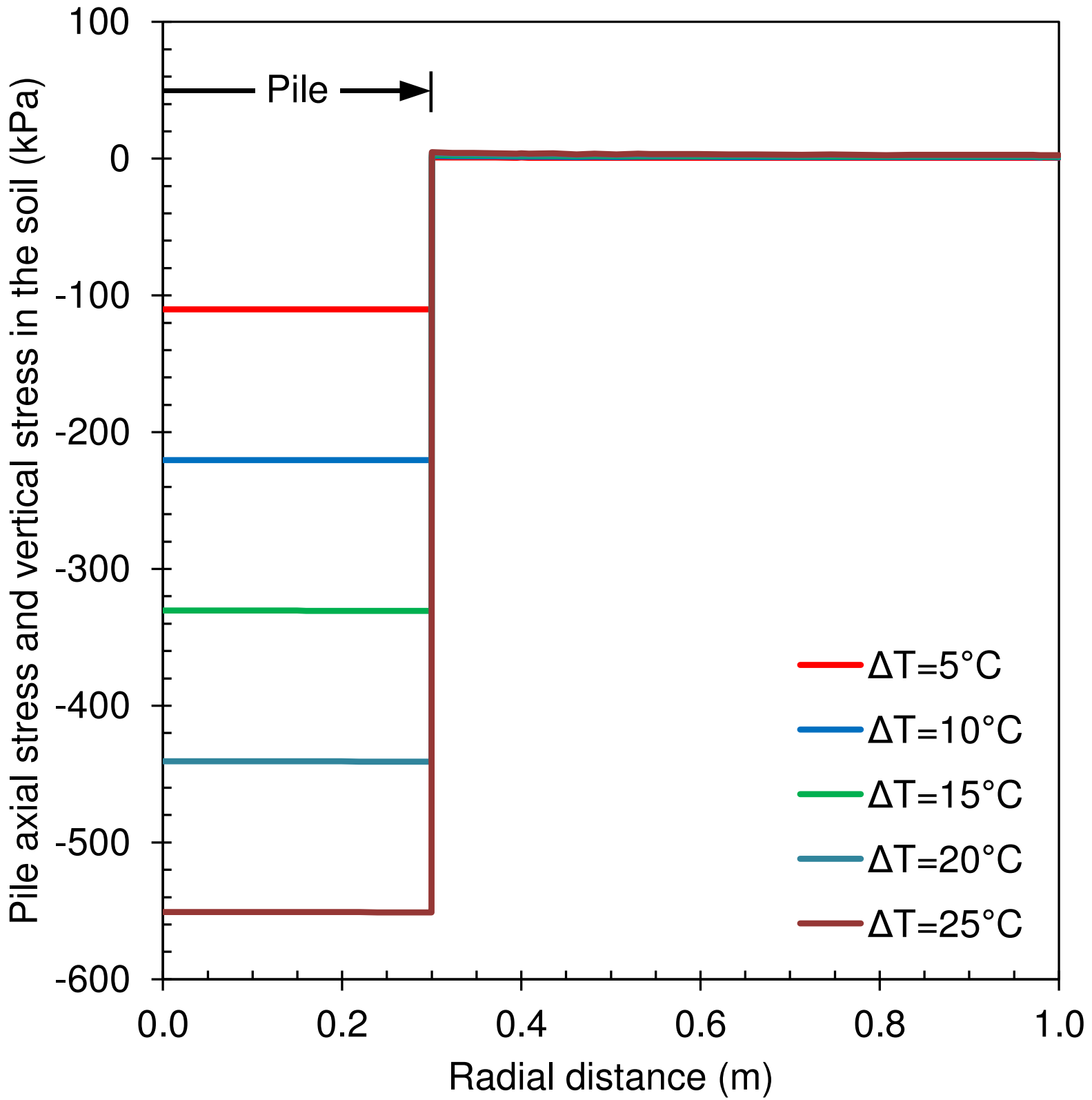


Figure 6
[Click here to download Figure: Fig 6.eps](#)

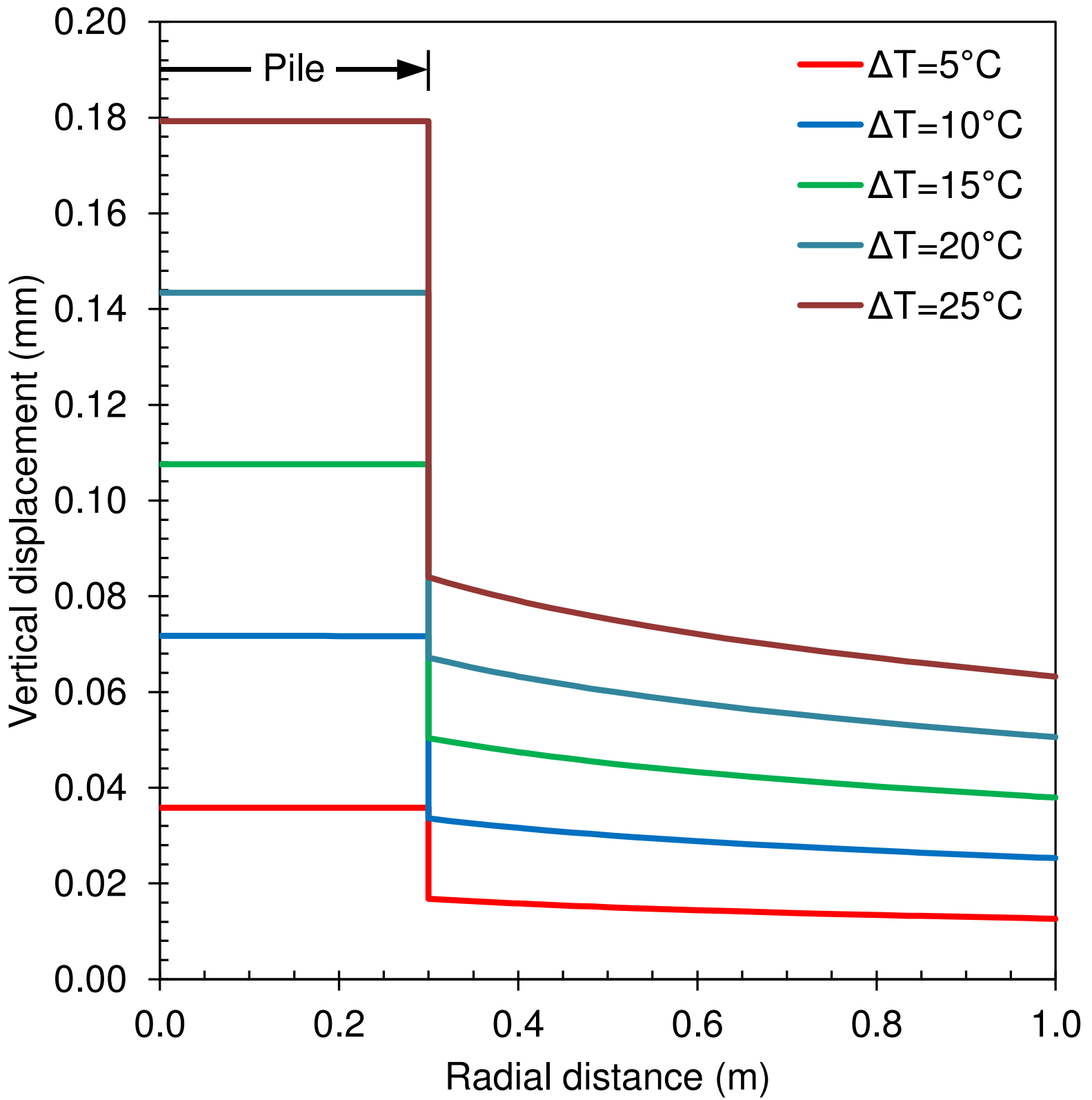


Figure 7
[Click here to download Figure: Fig 7.eps](#)

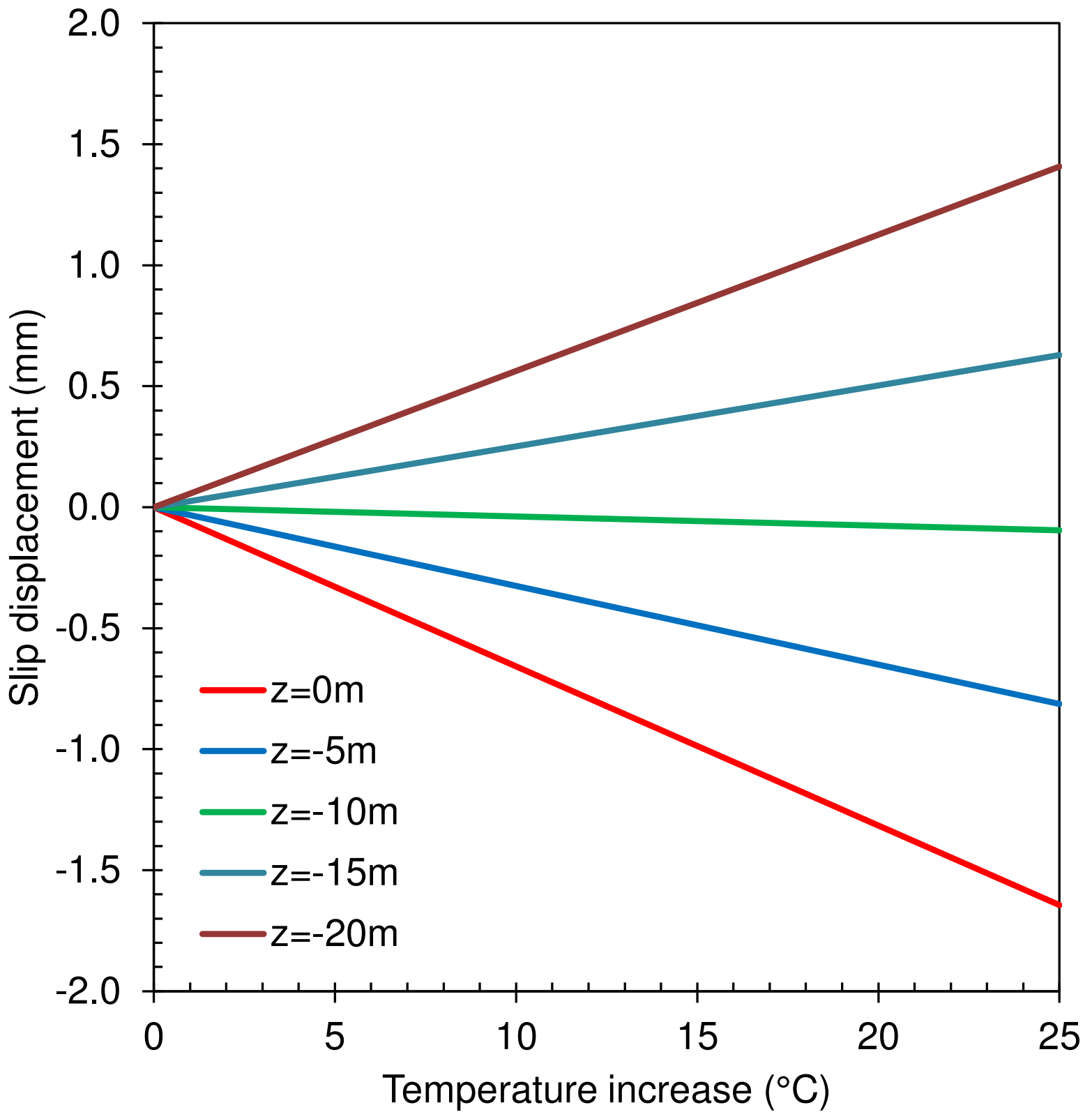


Figure 8
[Click here to download Figure: Fig 8.eps](#)

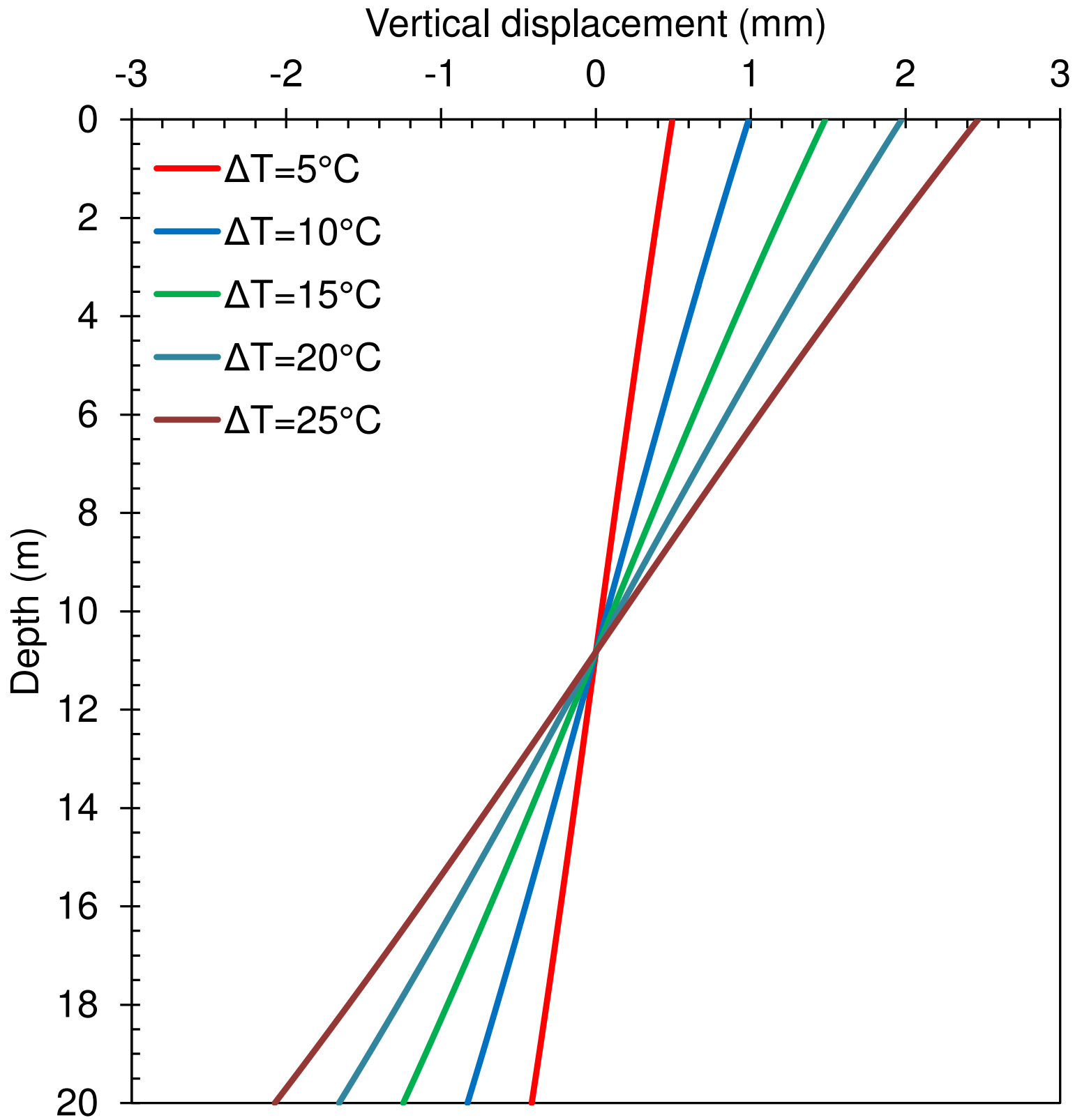


Figure 9
[Click here to download Figure: Fig 9.eps](#)

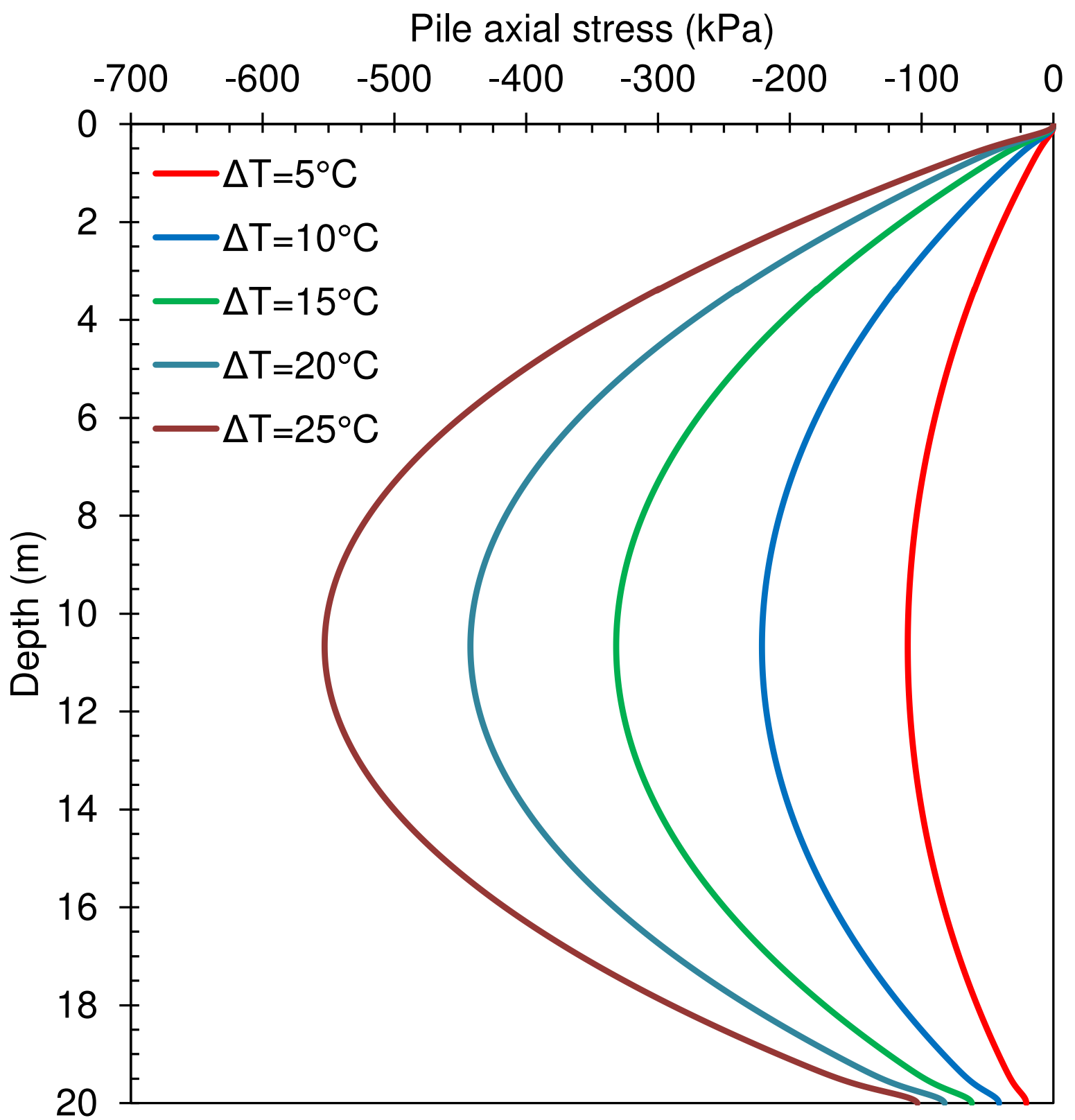


Figure 10
[Click here to download Figure: Fig 10.eps](#)

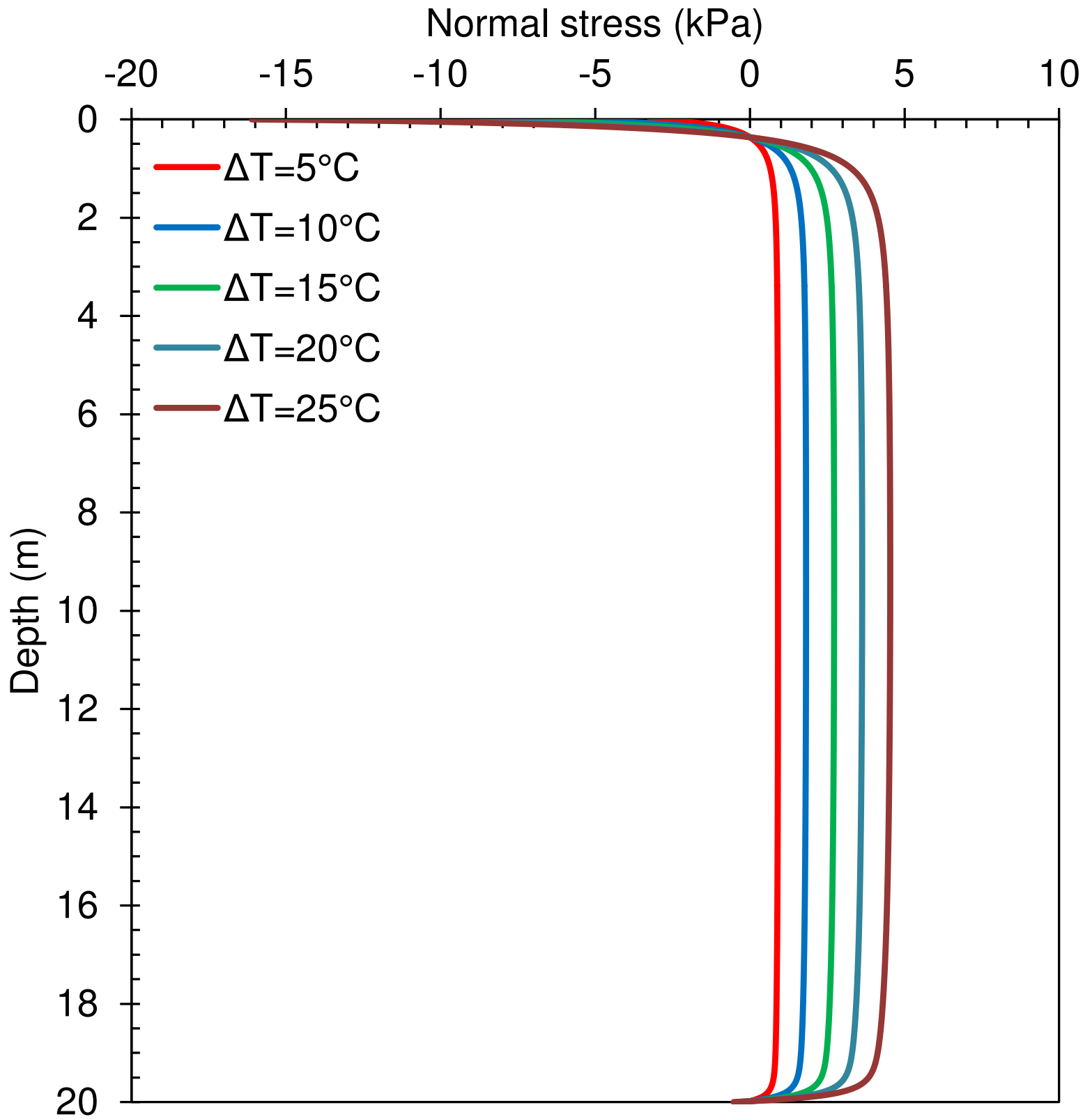


Figure 11
[Click here to download Figure: Fig 11.eps](#)

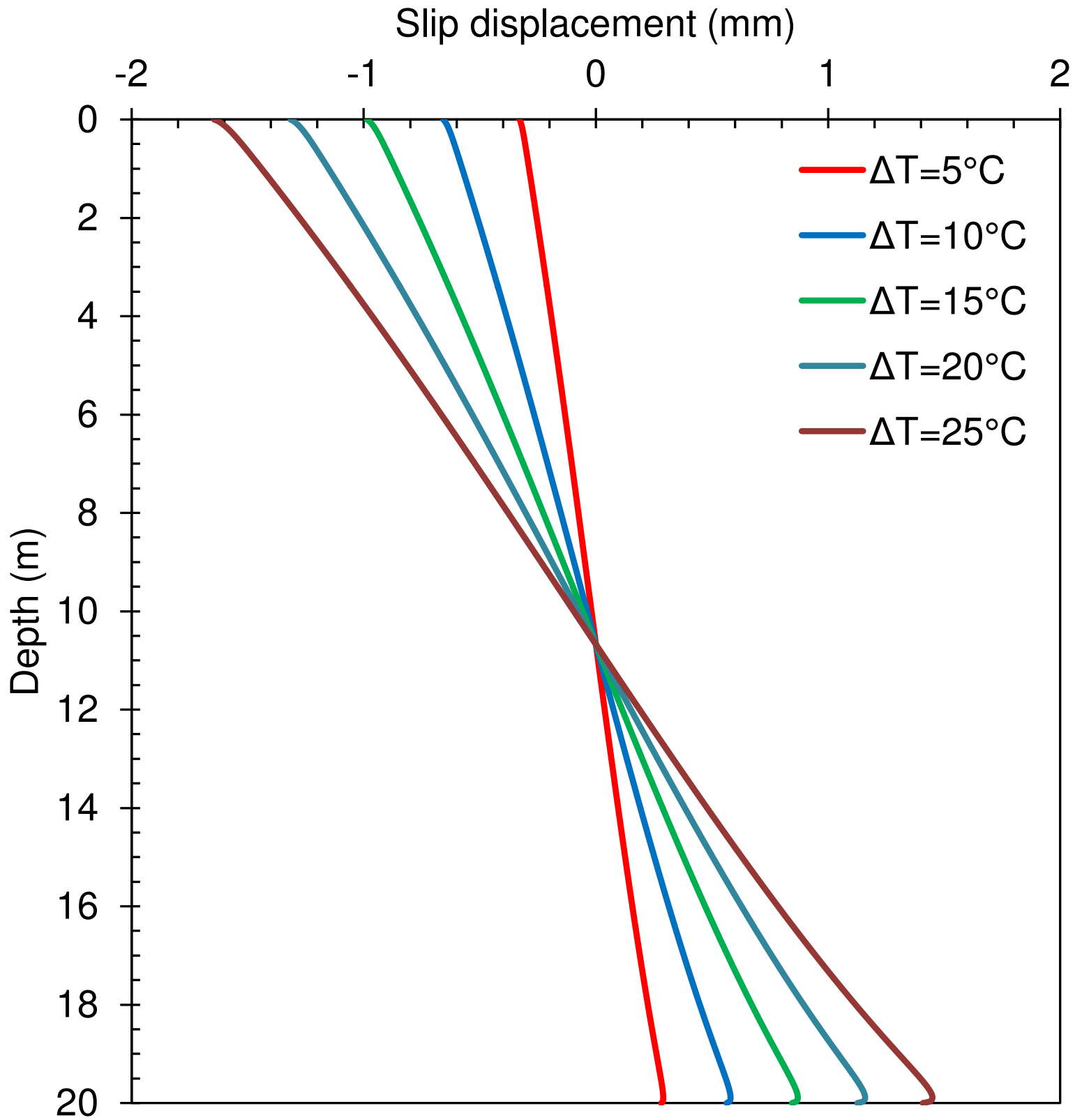


Figure 12
[Click here to download Figure: Fig 12.eps](#)

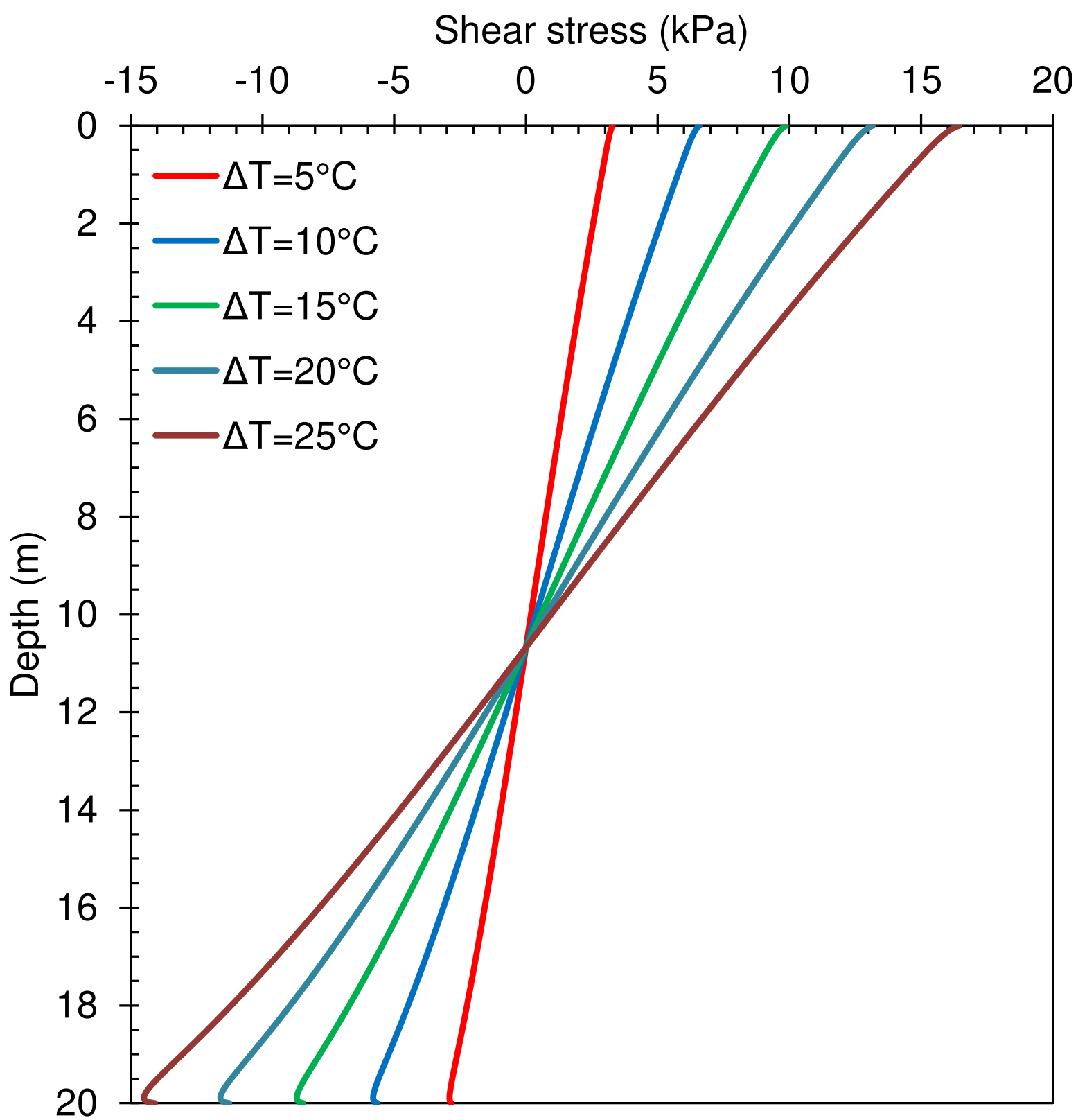


Figure 13
[Click here to download Figure: Fig 13.eps](#)

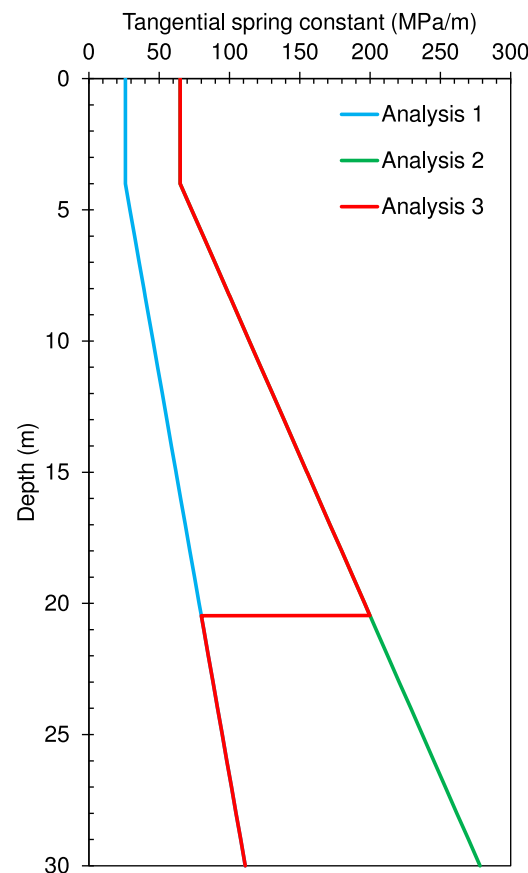
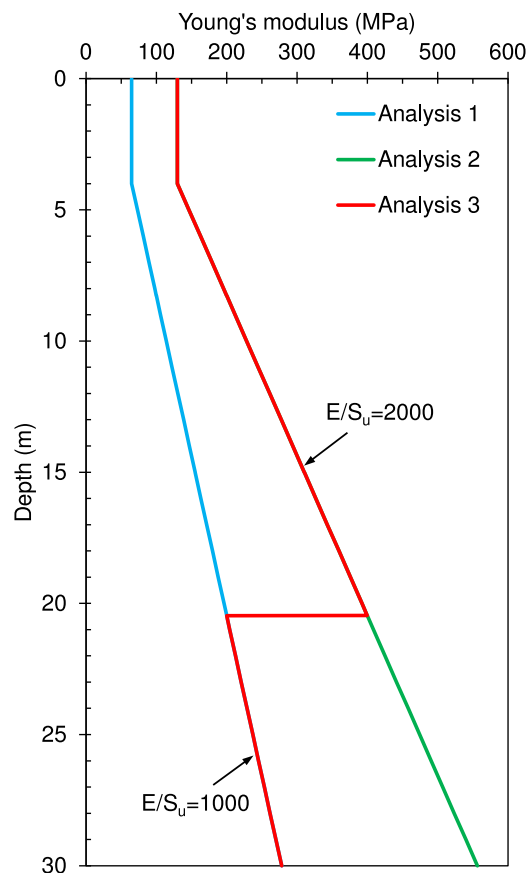
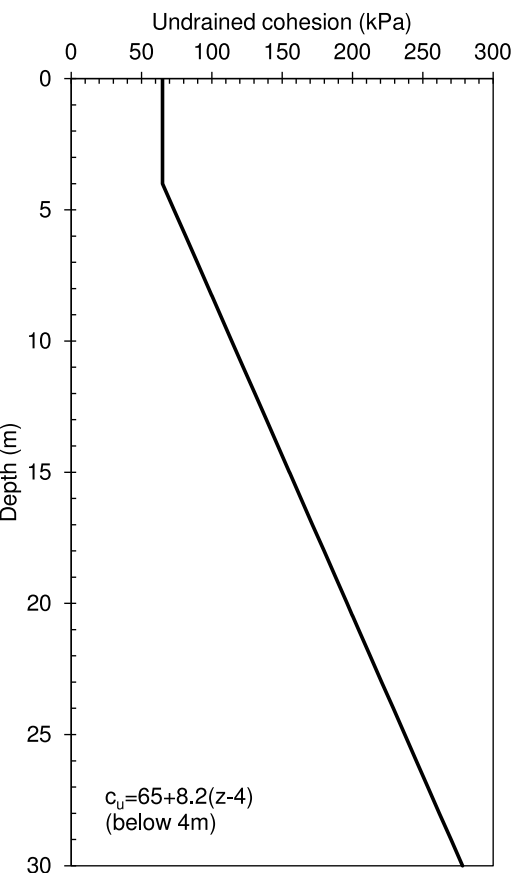


Figure 14
Click here to download Figure: Fig 14.eps

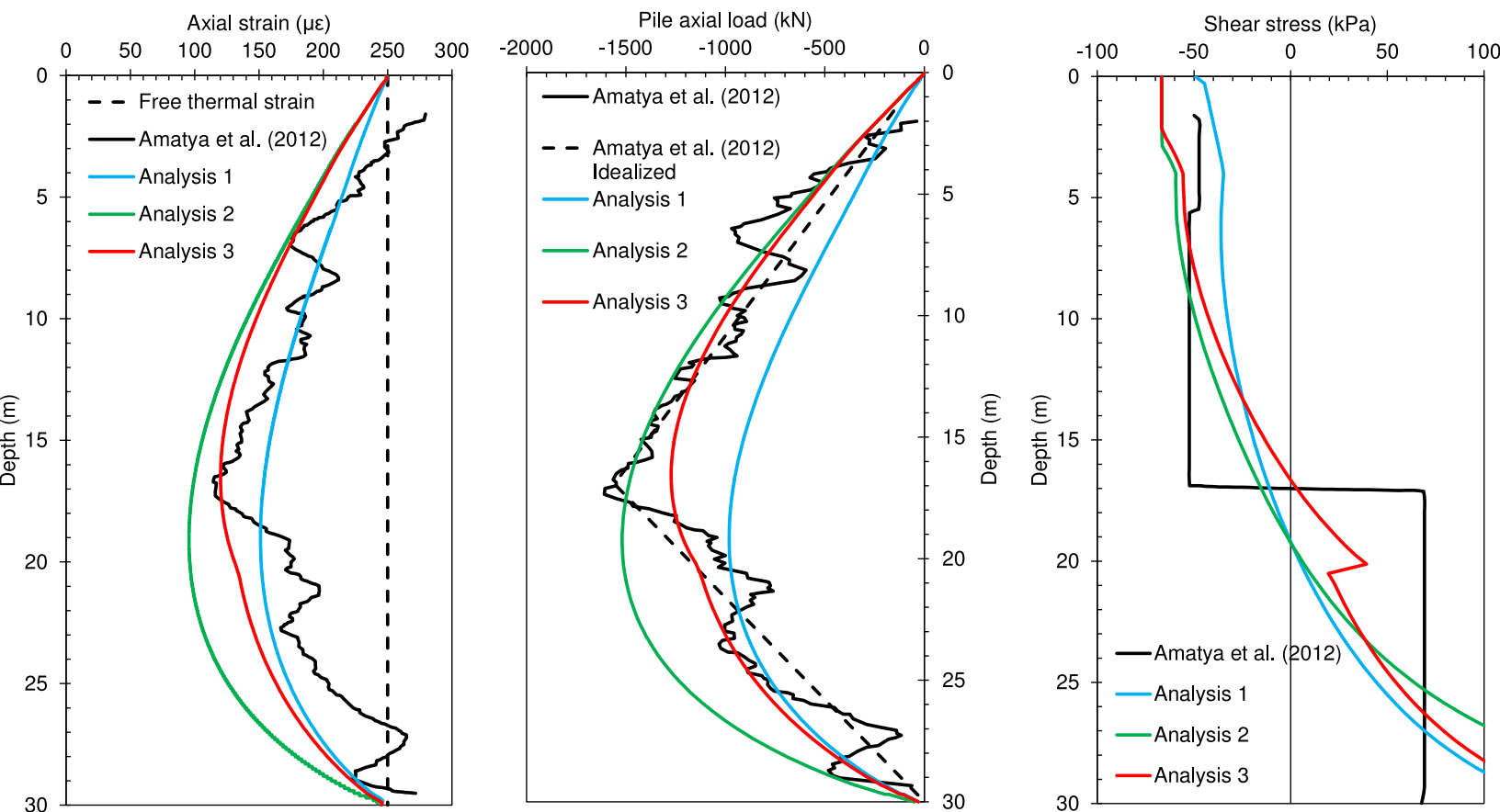


Figure 15
[Click here to download Figure: Fig 15.eps](#)

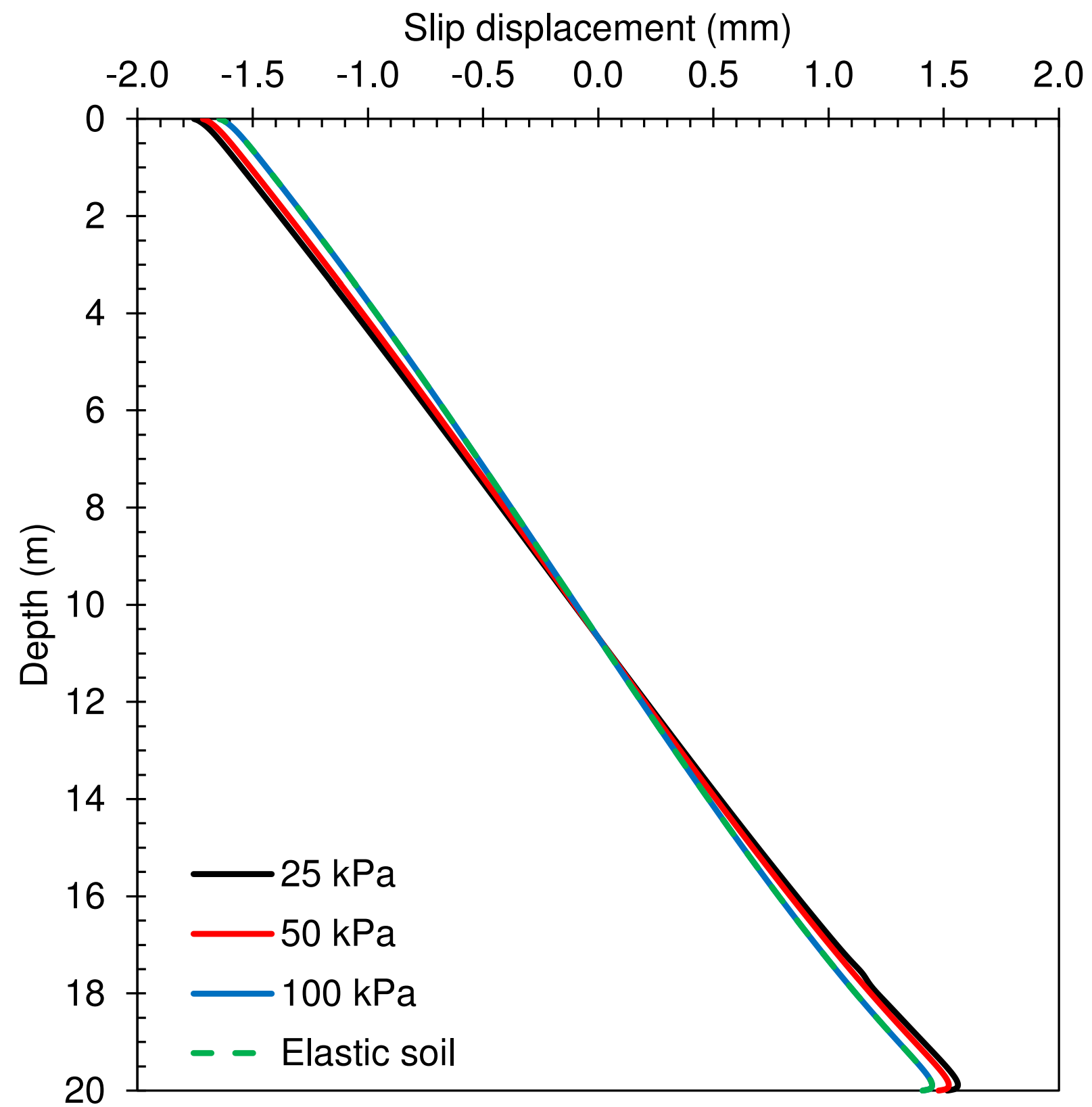


Figure 16
[Click here to download Figure: Fig 16.eps](#)

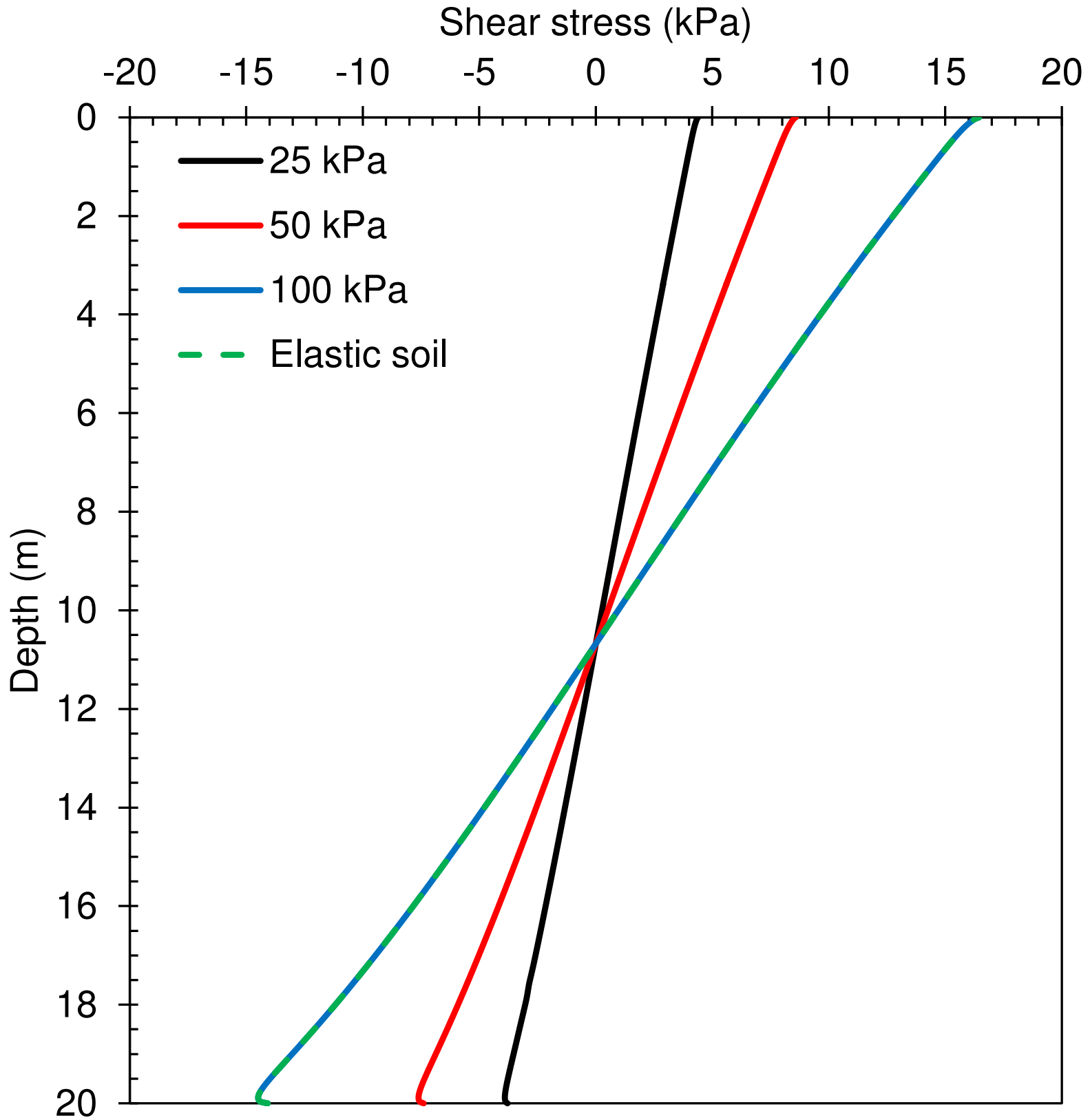


Figure 17
[Click here to download Figure: Fig 17.eps](#)

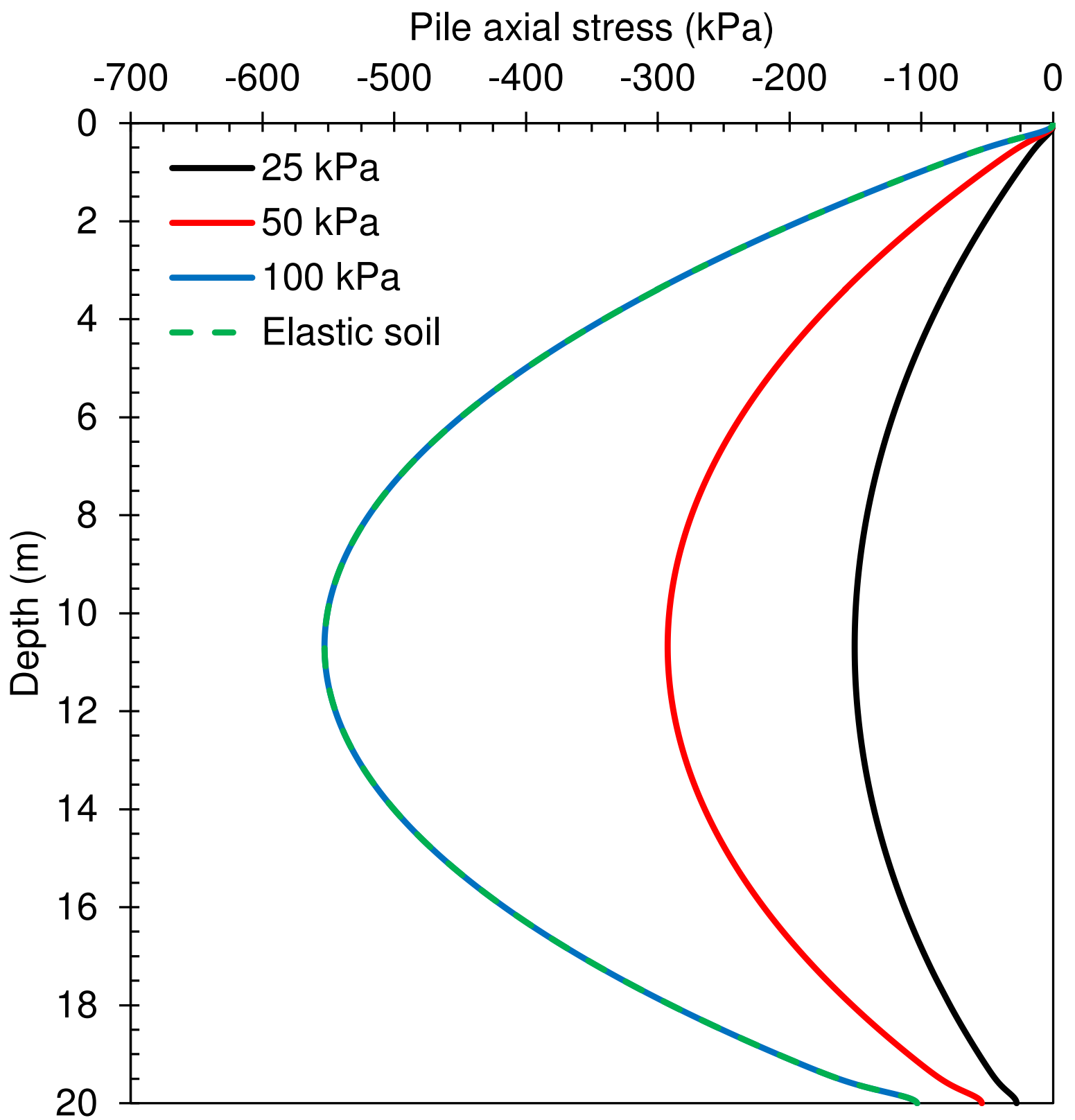


Figure 18
[Click here to download Figure: Fig 18.eps](#)

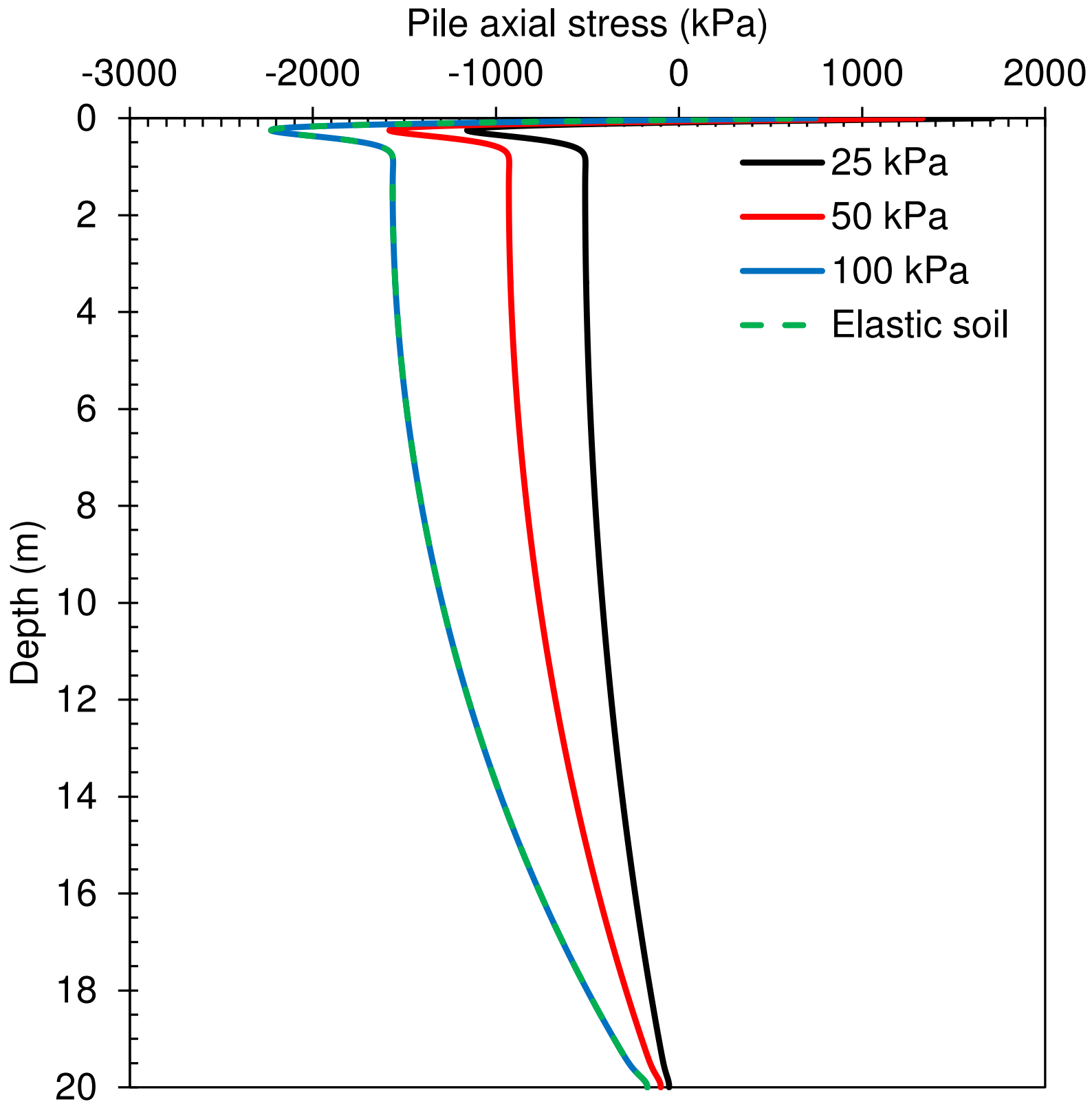


Figure 19
[Click here to download Figure: Fig 19.eps](#)

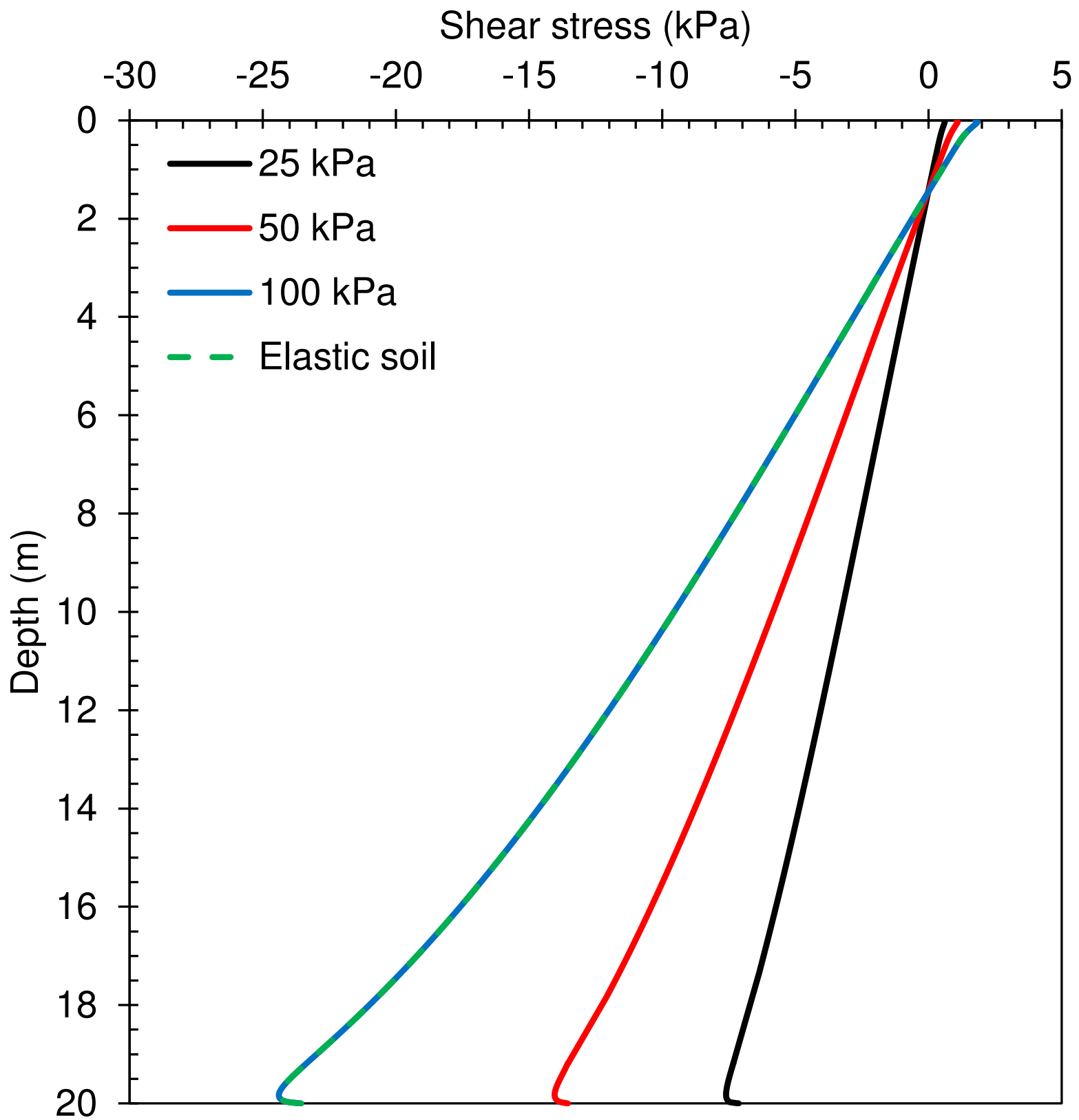


Figure 20
[Click here to download Figure: Fig 20.eps](#)

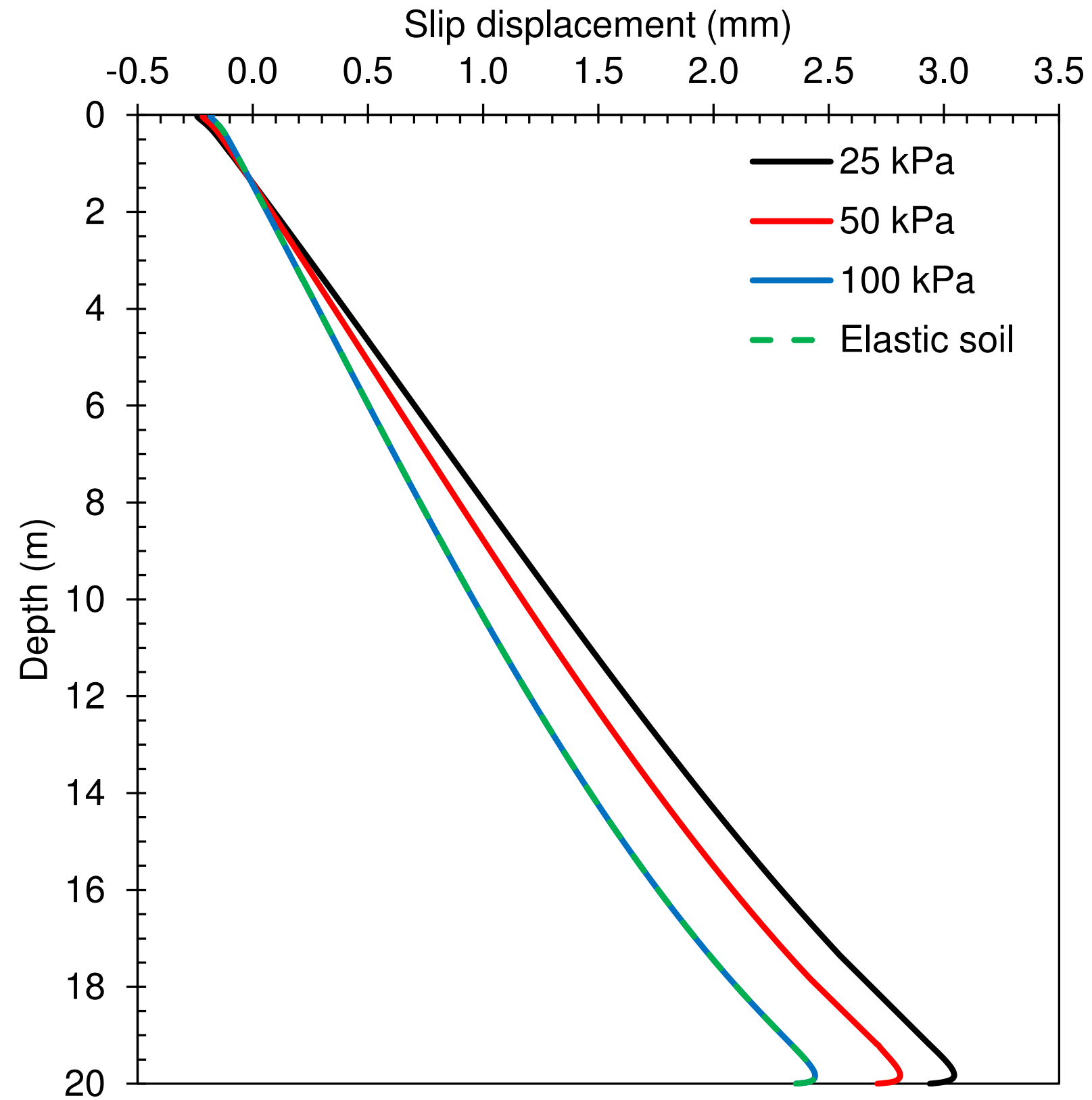


Table 1 Constitutive equations used in the numerical model for soil elements, concrete elements (in the heat exchanger pile) and the interface elements

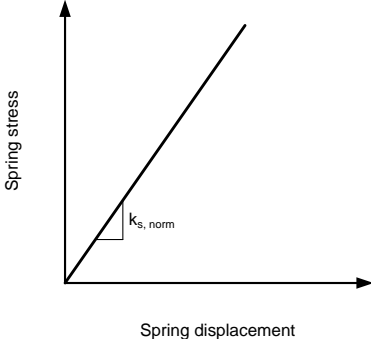
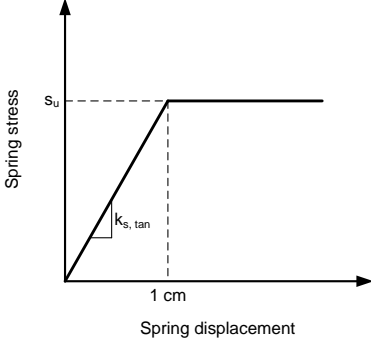
Soil	Mohr-Coulomb elastic-perfectly plastic model	$ \tau + \sigma \tan \phi - c = 0$
Concrete	Thermo-elastic model	$\sigma = \frac{E}{(1+\nu)} \varepsilon + \frac{\nu E}{(1+\nu)(1-2\nu)} Tr(\varepsilon) \delta$ $+ \frac{E}{3(1-2\nu)} \alpha \Delta T \delta$
Interface		$\sigma \cdot \mathbf{n} = -\mathbf{k}_s (\mathbf{u}_{pile} - \mathbf{u}_{soil})$
	Linear elastic normal contact law	
	Linear elastic-perfectly plastic tangential contact law	

Table 2 Material properties

Parameter / Material	Concrete	Soil
Mass density (kg/m ³)	2500	2000
Young's modulus (MPa)	17000	500 × s _u
Poisson's ratio	0.150	0.495
Thermal conductivity (W/(m·K))	1.5	–
Heat capacity (J/(kg·K))	1200	–
Coefficient of thermal expansion (με/K)	10	–
Cohesion (kPa)	–	25 / 50 / 100 / elastic
Angle of internal friction (°)	–	0

Table 3 Soil types and strength parameters

Parameter / Soil type	1	2	3	4
Cohesion (kPa)	25	50	100	–
Friction angle (°)	0	0	0	–
Young's modulus (MPa)	12.5	25.0	50.0	50.0
Poisson's ratio	0.495	0.495	0.495	0.495
Pile/soil tangential interface stiffness (MPa/m)	2.5	5.0	10.0	10.0
Pile/soil normal interface stiffness (MPa/m)	25.0	50.0	100.0	100.0

Table 4 Input parameters used in the analyses for model validation

Input parameter / Analysis #	Analysis 1	Analysis 2	Analysis 3
E/S_u	1000	2000	2000, $S_u \leq 200$ kPa 1000, $S_u > 200$ kPa
Slip displacement at fully mobilized shaft resistance (mm)	2.5	1.0	1.0, $S_u \leq 200$ kPa 2.5, $S_u > 200$ kPa